Simulating brittle and ductile response of alumina ceramics under dynamic loading

Simons, E. C.; Weerheijm, J.; Sluys, L. J.

DOI
10.1016/j.engfracmech.2019.05.013

Publication date
2019

Document Version
Accepted author manuscript

Published in
Engineering Fracture Mechanics

Citation (APA)
Simons, E. C., Weerheijm, J., & Sluys, L. J. (2019). Simulating brittle and ductile response of alumina ceramics under dynamic loading. *Engineering Fracture Mechanics*, *216*, 1-20. Article 106481. https://doi.org/10.1016/j.engfracmech.2019.05.013

Simulating brittle and ductile response of alumina ceramics under dynamic loading

E.C. Simons[a], J. Weerheijm[a,b], L.J. Sluys[a]

[a]*Delft University of Technology, P.O. Box 5048, 2600 GA Delft, The Netherlands*
[b]*TNO, P.O. Box 45, 2280 AA Rijswijk, The Netherlands*

Abstract

Alumina ceramic is often used in armour systems. This material is known to have a brittle response under tensile loading, while a ductile response is found when sufficiently high pressures are reached. During projectile impact a ceramic material experiences both tensile loading and high pressures, hence fails in both a brittle and ductile way. Properly capturing the ceramic failure in a single material model remains challenging. A viscosity regularized Johnson-Holmquist-2 model has been used to simulate dynamic loading on alumina ceramic. The simulations show that the brittle and ductile nature of the material can not be captured simultaneously in the current material model. A new failure strain formulation is proposed where the behaviour under tensile and compressive loading can be controlled independently. This allows to properly capture both the brittle and ductile response of the material in a single constitutive framework, with a single set of model parameters.

Keywords: ceramic, Johnson-Holmquist, ductile, brittle, failure

1. Introduction

Ceramic materials such as alumina and silicon carbide are widely used in armour systems. These ceramics have a high hardness and relatively low weight when compared to traditional armour materials such as steel. The high hardness of the ceramic ensures heavy deformation and even fracturing of incoming projectiles. The ceramic material itself may also damage during this interaction. As long as the ceramic can exert a force on the projectile, the deformation and deceleration of the projectile continues. Understanding the failure process of a ceramic material is therefore key in understanding the projectile/armour interaction [1, 2, 3]. Armour ceramics show multiple modes of failure. Under tension the behaviour is brittle, while a more ductile behaviour can be found under compression. The brittle nature under tensile loading is attributed to macro crack formation. While the ductile behaviour of the ceramics under compression can be explained by micro-crack formation and plasticity. Plastic deformation of ceramics under impact is well known and appears for sufficiently high confining pressures [4, 5, 6, 7, 8].

Although the main modes of failure are known for armour ceramics it is still difficult to properly capture their behaviour, the sequence of occurrence and the interaction of mechanisms with a computational model. Experimental measurements of the individual failure processes are very limited. True impact experiments with projectiles can be performed, but material behaviour is often deducted rather than measured. The latter is difficult due to highly varying stress states and the catastrophic nature of the experiments. There are two main paths one can take to better understand the failure process. The first way is to limit the loading rates, and therefore consider quasi-static indentation tests [9, 10] and slow dynamic testing such as drop-weight impact tests [7]. The main advantage of these tests is that the ceramic does not fail catastrophically. This makes it possible to examine intermediate stages of failure which lie between intact and fully failed. A second way to study ceramic failure is by simplifying the dynamic loading, e.g. by plate impact or spall tests. In these experiments the material is loaded in a well defined way, which makes it possible to deduct the material behaviour under these dynamic loading scenarios. When building a constitutive model for ceramics this type of information is essential. The main advantage of the second type of tests over the first one is that the dynamic nature of the impact problem is maintained, which is why the second approach is adopted in this paper.

Plate impact tests have been performed on ceramic materials over the past decades, providing a great deal of information in literature [11, 12, 13, 14, 15, 16, 17, 18, 19, 20]. In a plate impact experiment high pressures can be

Nomenclature

A	intact deviatoric strength parameter
B	residual deviatoric strength parameter
C	rate dependency parameter
d_1	deviatoric failure strain parameter
d_2	failure strain pressure dependency exponent
D	scalar damage variable
$\dot{D}$	rate of the scalar damage variable
E	Young's modulus
f	yield function
HEL	Hugoniot Elastic Limit
m	residual strength pressure dependency exponent
n	intact strength pressure dependency exponent
p	pressure
p_c	maximum failure strain threshold pressure
p_t	minimum failure strain threshold pressure
P_{HEL}	pressure at HEL
T	hydrostatic tensile strength
T_0	rate independent hydrostatic tensile strength
T_t	hydrostatic tensile strength for transition rate
$\boldsymbol{\epsilon}$	strain tensor
$\dot{\bar{\epsilon}}_0$	reference equivalent plastic strain rate
$\dot{\bar{\epsilon}}_p$	equivalent plastic strain rate
$\dot{\bar{\epsilon}}_p^*$	equivalent plastic strain rate normalized to $\dot{\bar{\epsilon}}_0$
$\bar{\epsilon}_p^f$	equivalent plastic failure strain
$\bar{\epsilon}_p^{f,min}$	minimum equivalent plastic failure strain
$\bar{\epsilon}_p^{min}$	minimum equivalent plastic failure strain
$\bar{\epsilon}_p^{max}$	maximum equivalent plastic failure strain
η	viscosity
$\dot{\lambda}$	rate of plastic multiplier
$\dot{\lambda}_t$	threshold rate of plastic multiplier
ν	Poisson's ratio
ρ	density
$\boldsymbol{\sigma}$	stress tensor
σ_{eq}	Von Mises equivalent stress
σ_{HEL}	equivalent stress at HEL
σ_i	intact deviatoric material strength
σ_f	residual deviatoric material strength
σ_i^*	intact deviatoric material strength normalized to σ_{HEL}
σ_f^*	residual deviatoric material strength normalized to σ_{HEL}
σ_y	yield stress
σ_y^*	yield stress normalized to σ_{HEL}
FE	Finite Element
JH2	Johnson-Holmquist-2
JH2-V	Viscosity regularized Johnson-Holmquist-2

reached and the material fails under compressive loading. The material is loaded in uniaxial strain and by measuring the free surface velocity of the impacted plate the stress wave inside the material can be reconstructed. This stress wave signal can then be used to derive material behaviour. Spall tests provide a second simplified loading scenario. Two types of spall tests can be performed, either a slender bar [21, 22, 23, 24] of ceramic or a wide plate [25, 26, 27] is loaded. Similar to plate impact a spall test performed on a plate will load the material in uniaxial strain conditions, but in the spall test the target material fails under tension.

The plate impact and spall tests provide good insight in the material behaviour under pure compressive or tensile loading. This information can be used to calibrate or validate a constitutive model. The constitutive model should be able to capture the behaviour of the ceramic for both tests. This means that the model should be able to capure the brittle and ductile behaviour under tension and compression. Multiple constitutive models for ceramics have been proposed in literature over the past decades. Noteworthy models are those by Johnson and Holmquist [28, 29, 30], Simha [31] and Deshpande-Evans [32, 33]. Most of the available ceramic material models are essentially softening plasticity models. The main difference lies in the description of the material strength and the way the models deal with ceramic failure. In the current paper the second model by Johnson-Holmquist [29] (JH2) is chosen as this is an often used and widely accepted ceramic material model for ballistic impact.

Softening plasticity models (such as the JH2 model) are well known to suffer from mesh dependency. In [34] a modification of the JH2 model was proposed which solved this mesh dependency. The modification consisted of the inclusion of rate dependency (i.e. viscosity) on the hydrostatic tensile strength of the material. Adding a viscosity to a constitutive model is known to provide an implicit length scale, which can regularize the solution and solve the mesh dependency problem [35, 36, 37]. In addition to providing mesh independency for the JH2 model results it was seen that the rate dependency of the tensile strength allowed the model to properly capture experimentally measured rate dependency of the spall strength of ceramic [26], where the original JH2 model failed to do so.

The goal of the current paper is to find a generic model, capable of simulating ceramic failure both under tension and compression, subjected to a range of loading rates. The viscosity regularized JH2 model (JH2-V) from [34] is used as a starting point. This model will be described in Section 2. In Section 3 the JH2-V model (and the original JH2 model) will be extensively tested. The models will be used to simulate a spall test, a plate impact tests, a spherical impact test and a quasi-static ring-on-ring bending test. For a correct material model all of these tests should give an adequate match between experiments and simulations, for a single set of model parameters. Unfortunately the analysis shows that this is not true for the JH2-V model (or the JH2 model). Fortunately the simulation results give a clear indication that this is related to the failure formulation of the model. The failure formulation in these models only allows for either brittle failure under tension or ductile failure under compression. This is because the damage rate in the failure formulation is a single pressure dependent function, coupling the behaviour under tension and compression through the model parameters. In section 4 the failure formulation is modified such that the failure response under tension and compression is separated. This allows independent control over the damage rate under tensile and compressive loading. Calibration of the new formulation is done based on spall and plate impact tests. It is shown that the JH2-V model with the new softening formulation can properly capture the ceramic's behaviour in all four considered loading scenarios, for a single set of model parameters.

2. Methods and Models

Finite element (FE) simulations are performed. For the FE simulations a C++ based code is used, developed with the open source FE libraries provided by JemJive[38]. Implicit solution schemes are used for the simulations in this paper, Newton-Raphson for the quasi-static simulations and Hilbert-Hughes-Taylor-α for the dynamic simulations.

The choice for this numerical framework will be briefly explained by two comments. First a comment on the FE method. This is a well established method to solve a partial differential equation (PDE). Other methods may also be used, such as the material point method (MPM) [39, 40], smooth particle hydrodynamics (SPH) [41, 42, 43, 44, 45] and many others. These methods may have some advantages and disadvantages over the FE method. One major advantage of MPM and SPH is that these mesh-less methods easily deal with large deformations, but they tend to be more computationally heavy than FEM. Since the test cases in the current paper do not experience large deformation the FE method remains a good choice. The second comment is on the choice for the implicit time integration scheme. Compared to explicit time integration schemes these implicit schemes have two main advantages. The first is that the balance of linear momentum is exactly satisfied in each time step, which is not true for explicit schemes. The second advantage is that these implicit schemes are unconditionally stable, and as such do not have a critical time step. This means time steps can be much larger than what is possible in explicit time integration schemes. This feature is further exploited in the current paper by using an adaptive time integration scheme, to keep the implicit scheme robust and fast. The Hilbert-Hughes-Taylor-α method furthermore has some damping included in its formulation, which may help when simulating dynamic contact problems [46]. The choice of how one solves the PDE and how one deals with time integration is independent of the material model. The constitutive model developed in the current paper should therefore be considered as a general model, not bound by the FEM or implicit time integration.

In the current paper the Johnson-Holmquist-2 [29] model is used, as this is a widely accepted material model for ceramics. The section will start with a short description of the material strength in this model, as well as the viscosity regularized formulation from [34]. The second part of the section will show how failure is captured in the ceramic material models JH2 and JH2-V, as well as several others.

2.1. Material strength

2.1.1. Johnson-Holmquist-2

In the Johnson-Holmquist-2 (JH2) model the yield function f of the material is described as

$$f(\boldsymbol{\sigma}, D) = \sigma_{eq}(\boldsymbol{\sigma}) - \sigma_y(\boldsymbol{\sigma}, D), \tag{1}$$

where $\boldsymbol{\sigma}$ is the stress tensor, D a scalar damage variable, σ_{eq} the Von Mises stress and σ_y the material strength. This material strength can be found as

$$\sigma_y^*(\boldsymbol{\sigma}, D) = (1 - D)\ \sigma_i^*(\boldsymbol{\sigma}) + D\ \sigma_f^*(\boldsymbol{\sigma}), \tag{2}$$

where * indicates that the values are normalized with respect to the equivalent stress at the Hugoniot elastic limit, i.e. σ_{HEL}. The material strength σ_y is an interpolation of the intact and residual strengths σ_i and σ_f with damage D. The intact and residual material strengths are a function of the pressure $p(\boldsymbol{\sigma}) = -\frac{1}{3}\sigma_{ii}$ and can be expressed as

$$\sigma_i^*(\boldsymbol{\sigma}) = A\left(\frac{T + p(\boldsymbol{\sigma})}{P_{HEL}}\right)^n \left(1 + C\ln\dot{\epsilon}_p^*\right), \tag{3}$$

$$\sigma_f^*(\boldsymbol{\sigma}) = B\left(\frac{p(\boldsymbol{\sigma})}{P_{HEL}}\right)^m \left(1 + C\ln\dot{\epsilon}_p^*\right). \tag{4}$$

Here A, B, C, n, m, T and P_{HEL} are material properties and $\dot{\epsilon}_p^*$ is the rate of equivalent plastic strain normalized with respect to reference rate $\dot{\epsilon}_0$. The rate dependency is controlled through parameter C. This rate dependency provides a deviatoric scaling of the material strength.

2.1.2. Johnson-Holmquist-2 Viscosity-regularized

In [34] a modification to the JH2 model was proposed. To solve mesh dependency of the original model an apex viscosity was introduced (hence Johnson-Holmquist-2 viscosity-regularized or JH2-V). The material strengths from (3) and (4) are now replaced by

$$\sigma_i^*(\boldsymbol{\sigma}) = A\left(\frac{T(\dot{\epsilon}_p) + p(\boldsymbol{\sigma})}{P_{HEL}}\right)^n, \tag{5}$$

$$\sigma_f^*(\boldsymbol{\sigma}) = B\left(\frac{p(\boldsymbol{\sigma})}{P_{HEL}}\right)^m. \tag{6}$$

In this formulation the apex pressure T is now a function of rate, providing a rate dependent tensile strength to the material. In the above formulations the original logarithmic rate dependency is absent, however the new formulation does not exclude the original formulation as both formulations may be used together.

The proposed apex viscosity is a mixed linear/logarithmic formulation

$$T(\dot{\epsilon}_p) = T(\dot{\lambda}) = \begin{cases} T_0 + \eta\dot{\lambda} & \text{for } \dot{\lambda} < \dot{\lambda}_t, \\ T_t\left(1 + \frac{\eta\dot{\lambda}_t}{T_t}\ln\left(\frac{\dot{\lambda}}{\dot{\lambda}_t}\right)\right) & \text{else.} \end{cases} \tag{7}$$

Here, λ is the rate of plastic multiplier, which is equal to the rate of equivalent plastic strain when using a deviatoric plastic flow rule. Furthermore, T_0 is the rate independent apex pressure, η is the viscosity and $\dot{\lambda}_t$ is the threshold rate for which the viscosity changes from linear to logarithmic. A transition pressure $T_t = T_0 + \eta\dot{\lambda}_t$ is also used in the formulation. The mixed linear/logarithmic formulation was found to provide mesh-independent results. In addition it was shown that the proposed viscosity formulation could match experimentally measured rate dependency of the spall strength of ceramics. The original strength formulation of the JH2 model failed to have mesh-independent results and also failed to capture the rate dependency in the spall strength.

2.2. *Ceramic softening*

A strength reduction in the JH2 and JH2-V models is achieved by the damage parameter D, as is shown in (2). This single damage parameter should be able to properly describe the underlying failure phenomena. This may be challenging since the failure behaviour of a ceramic under tension and compression can be very different. In this subsection damage growth of the JH2 model is compared to other models.

2.2.1. *Johnson-Holmquist-2*

In the JH2 model failure is a gradual process, where the yield stress reduces as the damage parameter D grows (as shown in (2)). The rate of damage is found as

$$\dot{D} = \frac{\dot{\bar{\epsilon}}_p}{\bar{\epsilon}_p^f}, \tag{8}$$

where $\dot{\bar{\epsilon}}_p$ is the rate of equivalent plastic strain and $\bar{\epsilon}_p^f$ is the plastic failure strain, for which the material is fully failed. The failure strain is not constant in the JH models but follows

$$\bar{\epsilon}_p^f(\boldsymbol{\sigma}) = d_1 \left(\frac{T + p(\boldsymbol{\sigma})}{P_{HEL}} \right)^{d_2}, \tag{9}$$

where d_1 and d_2 are material constants. The values of d_1 and d_2 are typically unknown for a ceramic, because direct measurement of plastic failure strain in ballistic experiments is currently impossible. The functional form of the failure strain formulation in (9) is therefore an assumption and the parameters are determined through inverse modeling. Table 1 lists some of the failure related properties used in literature when modeling alumina ceramic. The material density is added to give insight in the type of alumina ceramic considered in these sources. The difference between highest and lowest values for d_1 and d_2 is found to be one order of magnitude. This great diversity is a clear indication of their level of uncertainty.

Table 1: *JH2 failure strain constants for alumina ceramics*

d_1	d_2	ρ $[kg/m^3]$	source
0.002	0.83	3625	[47]
0.005	0.83	3625	[48]
0.005	1.00	3700	[49]
0.010	1.00	3800	[50]
0.001	1.00	3890	[51]
0.010	0.07	3890	[52]
0.0125	0.70	3890	[53]

In the JH2 formulation the failure strain for $p < T$ is zero and failure is instantaneous. In the JH2-V model the rate dependent material strength allows for the material to reach $p < T$. However, if the JH2 failure strain is used this will still result in sudden failure. Tensile failure in ceramic material is related to fracture and thus crack propagation. Crack propagation is known to occur at a finite and limited velocity. This argues against the sudden failure found in the JH2 softening formulation. A simple modification can be made to (9) to ensure a finite rate of damage and at the same time allow pressure beyond the apex pressure. The failure strain formulation is changed to read

$$\bar{\epsilon}_p^f(\boldsymbol{\sigma}) = \max\left(d_1 \left(\frac{T + p(\boldsymbol{\sigma})}{P_{HEL}} \right)^{d_2}, \bar{\epsilon}_p^{f,min} \right), \tag{10}$$

where $\bar{\epsilon}_p^{f,min}$ is a small but non-zero failure strain value. Please note that this is not the 'modified formulation' of the failure strain as mentioned in the introduction. Equation (10) is merely a fix to allow the failure strain to exist for pressures below the apex pressure. This is the formulation used to perform the initial comparative analyses in Section 3. Later in Section 4 a completely new failure strain formulation will be proposed to improve the model results.

2.2.2. Other ceramic models

The way the JH2 model deals with a reduction of strength is not unique. There are other softening plasticity models for ceramics which use similar approaches. For instance the closely related Johnson-Holmquist-1 (JH1) and the Johnson-Holmquist-Beissel (JHB) model, as presented in [28] and [30], respectively. These models use the same damage parameter as the JH2 model. However, the gradual interpolation of the material strengths is not present in the JH1/JHB models. Instead, for these models an intact strength is maintained until full failure is reached at $D = 1.0$, at which there is a sudden transition to the residual strength. This approach essentially means that the ceramic behaves perfectly plastic, with one sudden reduction of strength as full damage is reached.

Another approach is found in the Deshpande-Evans-2 (DE2) model [33]. In this model there are three distinct failure mechanisms incorporated. Depending on the triaxiality $\zeta = \sigma_m/\sigma_e$, with mean stress σ_m and equivalent stress σ_e, cracks grow: in pure tension, in tension/shear or do not grow. In this model the rate of damage increases as the stress state is closer to hydrostatic tension. Also interesting to note is that a hardening response is found for high compressive stress states.

A third approach is found in the material model by Simha [31]. In this model again three domains are identified, based on the principal stress in the material. The rate of damage is then determined by the number of principal stresses in tension, as well as the magnitude of the largest principal tensile stress. The difference between damage rate for compression and hydrostatic tension is even in the order of 10^4.

3. JH2-V model analysis

In the previous section multiple models for the failure behaviour of ceramics have been presented. In the current section the JH2-V model with the original JH2 failure strain formulation from (10) is examined. The model is validated with four different experimental tests: Spall, plate impact, spherical impact and quasi-static ring-on-ring bending. If the JH2-V material model is valid, it should be able to match experimental results in all four tests, for a single set of model parameters. This thorough analysis is meant to challenge and critically analyze the current material model. It will reveal shortcomings of the material model. Based on the analysis in the current section an improved model will be proposed in Section 4.

One comment should be made in advance regarding the experiments in this section. The experimental results are obtained from literature. These experiments have all been performed on a similar high purity alumina ceramic. In an ideal scenario they should have been performed on the exact same material, but unfortunately no such data set is available. Small variations in the material properties are therefore expected and have to be accepted.

3.1. Spall simulations

Spall experiments on plate material are typically performed by impact. One plate of material is given an initial velocity (the "impactor") and impacts a plate of the same material (the "target"), as is shown in Figure 1. The impacting plate generates a shockwave, which can lead to spall failure in the target material. The free surface velocity of the target plate can be measured to determine the spall strength of the material. Given that the lateral dimensions of the plates are much larger than the thickness, the central part of the plate experiences uniaxial strain. The problem can thus be simplified to a single column of material, with an axial velocity applied to the bottom surface. This is also shown in Figure 1, by the red dashed box.

Spall experiments on AL23 high purity alumina ceramics have been performed by Forquin's group [26]. These spall experiments were performed on alumina plates, but the stress wave was induced through an electromagnetic device rather than impact. This allows for the generation of a more controlled stress wave, or as the authors state a "shockless" spalling. In an earlier paper this experiment was simulated using the JH2 and JH2-V material models [34]. It was found that the original JH2 model with or without rate dependency fails to capture the rate effect under tension,

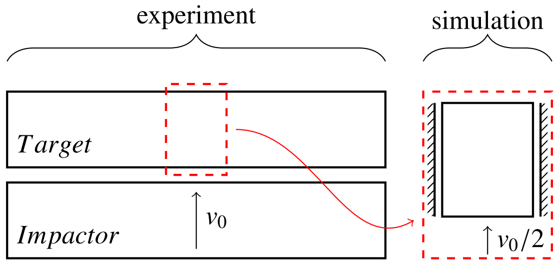

Figure 1: *Plate impact experiment and simplified model. Due to the axial loading nature the problem can be simplified to a column of material, subjected to some applied velocity on its lower edge. In plate impact the impactor arrives with initial velocity v_0 and impacts on the target material, generating $v(t) = 0.5v_0$ if both materials are the same. Methods other than impact can also be used to apply a velocity profile, such as the "shockless spall" method from [26].*

while the JH2-V model is able to capture the rate dependency measured in the spall strength of alumina ceramic. The current section briefly describes the simulations and results for the JH2-V model. The material properties from Table 2 in the column 'Spall value' are used in the simulations. These properties are based on [26], complemented by typical alumina values for the JH2 model from literature. Note that a minimal failure strain is imposed through equation (10) to allow a pressure below the (static) apex pressure T.

The spall test is simulated as a 10mm long and 2.5mm wide column, using linear three noded triangular elements under plane strain. The mesh is unstructured with element size $h \approx 0.1$mm. A velocity is prescribed on the bottom of the column, while the top remains free to move. As mentioned before, the sides of the column are constrained from lateral movement. The applied velocities in the experiments are known. Idealized applied velocity profiles are presented in Figure 2a, which are the velocities applied in the simulations.

The predicted spall strength as a function of rate is shown in Figure 2b. The spall strength is defined as the highest axial stress found when apex failure is first experienced. The rate is the total axial strain rate experienced by the point of maximum stress at this moment. From the graph it is clear that a viscosity formulation with $\eta = 0.028 \cdot 10^{-3}$ GPa·s and $\dot{\lambda}_t = \infty$ is sufficient to capture the rate effect of the spall strength. For $\eta = 0.000$ GPa·s the rate independent JH2 formulation is retrieved. It can be seen that this model fails to capture the rate dependency. The rate independent model results are similar to the stress at which a yield surface is reached under tension, which is the 'theoretical' strength in Figure 2b.

Figure 3 holds both the experimental and numerical predicted failure in the spall tests. Experimentally the ceramic could only be recovered from a single test. In this test the material was subjected to a wave similar to wave 2 from Figure 2a. The failure zones predicted in both simulations agree well with the experiment. The JH2-V model with zero viscosity shows a discrete failure pattern, typical for a material model suffering from mesh dependency. The viscous JH2-V model shows a more smooth damage profile, with intermediate values between intact and fully failed. Furthermore the viscous case shows damage extending beyond the experimentally observed failure zone. Whether this is also the case in the experiment is unknown, but the simulations performed in [26] also show non-zero crack densities beyond the cracked zone.

3.1.1. Spall - concluded

The spall simulations show that the rate dependent apex pressure in the JH2-V model allows to capture the rate effect under tension. The JH2 model fails to do so. This means that the apex viscosity is not only beneficial for regularization purposes, but it is also required in order to capture the (physical) rate dependent tensile strength.

3.2. Plate impact simulations

The spall simulations from the previous section show that the viscosity regularized JH2 model works well for alumina ceramics. The spall strength as a function of loading rate could be captured and (as far as experimental data are available) the failure zone was also found to be correct. In the current section the material is tested under compressive loading. Again a plate impact experiment is simulated, this time with a sufficiently high stress to cause failure under compression.

Table 2: *JH2-V material properties used in simulations, based on [26] and complemented by typical alumina values for the JH2 model from literature. The initial model values are found in the column 'Spall value'. Modified parameter sets are found in the other columns, where bold face notation is used for the parameters different from the spall value.*

variable	unit	Spall value	Plate impact value	variation 1 value	variation 2 value	variation 3 value	variation 4 value
E	GPa	360.0	**380.0**	**380.0**	**380.0**	**380.0**	360.0
ν	-	0.22	0.22	0.22	0.22	0.22	0.22
ρ	kg/m^3	3850	**3890**	**3890**	**3890**	**3890**	3850
A	GPa	0.930	0.930	0.930	0.930	0.930	0.930
B	GPa	0.310	0.310	**0.810**	0.310	0.310	0.310
n	-	0.6	0.6	0.6	0.6	0.6	0.6
m	-	0.6	0.6	0.6	0.6	0.6	0.6
C	-	0.0	0.0	0.0	0.0	0.0	0.0
T	GPa	0.2	0.2	0.2	0.2	0.2	0.2
η	GPa·s	$0.028{\cdot}10^{-3}$	$0.028{\cdot}10^{-3}$	$0.028{\cdot}10^{-3}$	$0.028{\cdot}10^{-3}$	$0.028{\cdot}10^{-3}$	$0.028{\cdot}10^{-3}$
$\dot{\lambda}_t$	s^{-1}	∞	∞	∞	$\mathbf{4 \cdot 10^4}$	$\mathbf{4 \cdot 10^4}$	∞
HEL	GPa	6.25	6.25	6.25	6.25	6.25	6.25
P_{HEL}	GPa	3.50	**3.25**	**3.25**	**3.25**	**3.25**	3.50
σ_{HEL}	GPa	4.125	**4.50**	**4.50**	**4.50**	**4.50**	4.125
d_1	-	0.005	0.005	0.005	**0.050**	**0.500**	**0.500**
d_2	-	0.75	0.75	0.75	0.75	0.75	0.75
$\bar{\epsilon}_p^{f,min}$	-	$1.5 \cdot 10^{-4}$	$1.5 \cdot 10^{-4}$	$1.5 \cdot 10^{-4}$	$1.5 \cdot 10^{-4}$	$1.5 \cdot 10^{-4}$	$1.5 \cdot 10^{-4}$

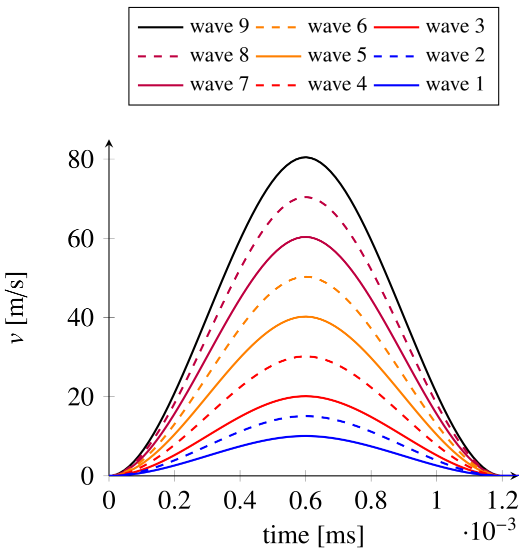

(a) *Applied velocity to induce a stress wave in the spall simulations.*

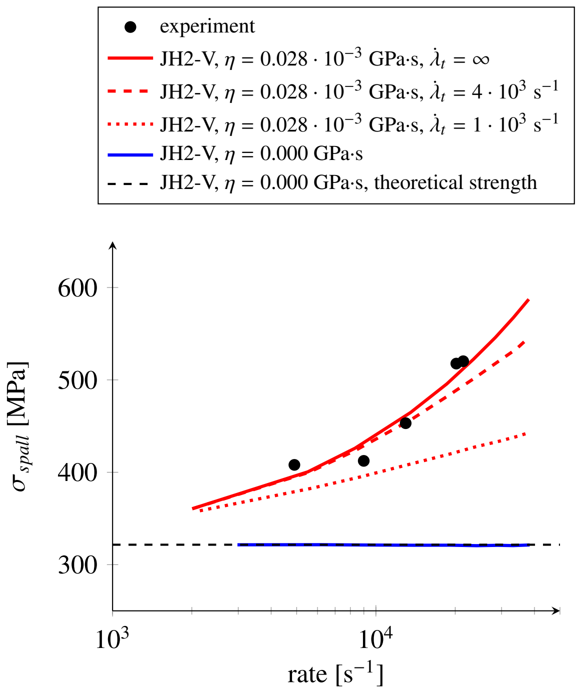

(b) *Spall strength, experimentally measured and predicted by simulation. Without viscosity the JH2-V model is not able to capture the rate dependency, but it gives a good match with experiments when* $\eta = 0.028 \cdot 10^{-3}$ *GPa·s and* $\dot{\lambda}_t = \infty$ *are used.*

Figure 2: *Spall test on alumina ceramic, comparing experiments to simulations.*

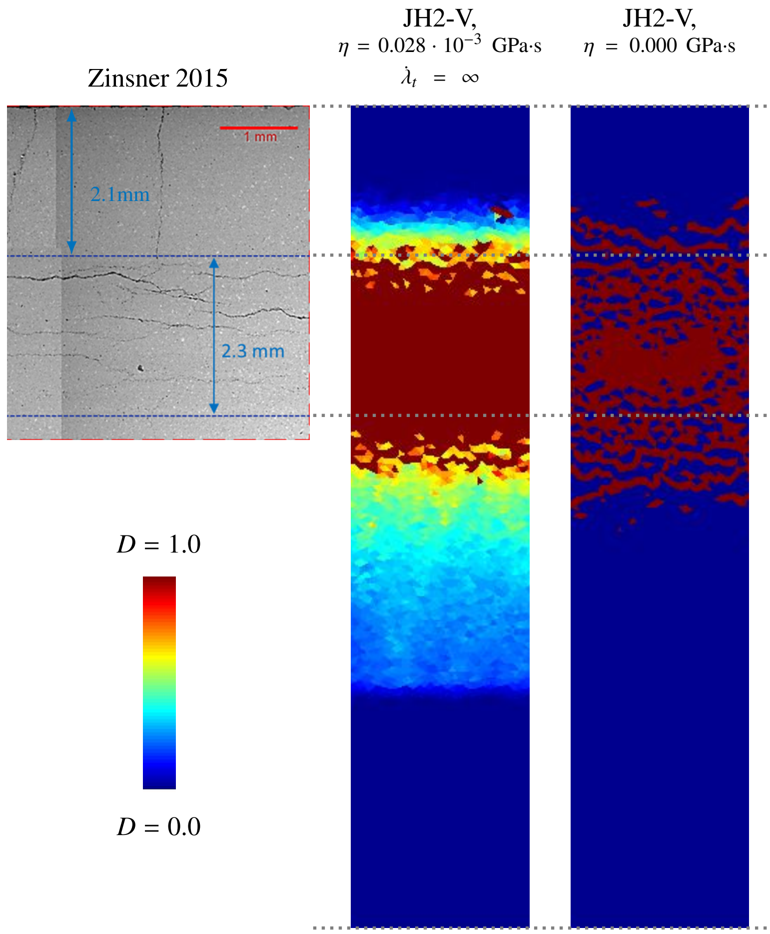

Figure 3: *Damage profiles obtained in the spall experiment [26] and FE simulations. Stress wave 2 from Figure 2a is applied. The JH2-V material model with and without viscosity is compared.*

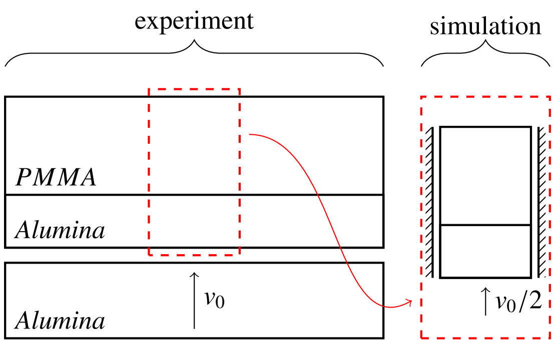

Figure 4: *Plate impact experiment and simplified model. The alumina target material is backed by a PMMA plate. Due to the axial loading nature the problem can be simplified to a column of material, subjected to an applied velocity on its lower edge. In plate impact the impactor arrives with initial velocity v_0 and impacts on the target material, generating $v(t) = 0.5v_0$ if both materials are the same. Please note that the true thickness ratios are different from those depicted here.*

In [54] results are reported for plate impact experiments on an aluminium oxide AD995, manufactured by the Coors Porcelain corporation. In these experiments a 5mm thick alumina flyer plate was given an initial velocity v_0. This flyer plate impacted a 10mm thick alumina target, which was backed by 25.4mm thick PMMA material. The impact velocity was such that the ceramic material failed under compression. The PMMA material was transparent, which allowed for a velocity measurement of the interface alumina/PMMA. This velocity signal at the interface contains information on the inelastic material behaviour. A schematic overview of the experiment is shown in Figure 4.

The plate impact experiment is simulated as a single column of four noded quadrilateral plane strain elements elements, with the JH2-V material model. A constant element size $h = 0.01$mm is used to mesh the column. A mixed Gauss integration scheme is used, where 2*2 integration is used for the deviatoric terms and 1 point integration for the hydrostatic terms [55]. Similar to the spall simulations the lateral movements of this column are constrained, while axial motion is allowed. The flyer plate is not modeled, instead a sudden velocity is applied on the target ceramic with a magnitude of half the flyer plate velocity. This generates a sudden shock wave in the ceramic target material, which will propagate as a stress wave. This idealized plate impact experiment is also shown on the right side in Figure 4.

The plate impact experiments in [54] report a material density of 3890kg/m3, which is slightly higher than what was used in the spall experiments (i.e. 3850kg/m3). Also the material stiffness is higher, 380GPa in the plate impact and 360GPa for the spall test. It is important to correct these values as they affect the wave speed in the material, which will in turn affect the interface velocity measurement obtained from the plate impact test. When changing the elastic properties the shock related P_{HEL} and σ_{HEL} should also be modified, as these quantities are related to the HEL of the material through the elastic constants. In the spall and plate impact experiments $HEL = 6.25$GPa, which gives $P_{HEL} = 3.25$GPa and $\sigma_{HEL} = 4.5$GPa for the modified material stiffness. The full parameter set with modified values can be found in the column 'Plate impact' from Table 2.

Figure 5 shows the experimental and numerical results for plate impact. The graph shows the velocity as a function of time, measured at the ceramic/PMMA interface. The dotted lines show the experimental results while the solid lines are used for the simulation results. An elastic stress wave arrives at the interface at point "A" in the graph. The velocity is found to rapidly rise to point "B". At this point the material behaviour changes from elastic to inelastic. This point is referred to as the Hugoniot elastic limit (HEL) of the material. After reaching the HEL the velocity continues to rise until a maximum velocity is reached at "C". The behaviour between points "B" and "C" will be referred to as the post-HEL behaviour. This post-HEL behaviour holds information on the ceramic strength during inelastic deformation. After reaching point "C" the velocity remains constant until the material experiences unloading at "D". This unloading is caused by wave reflection on the free surface of the flyer plate. In the simulations the focus lies on the loading behaviour (post-HEL, from "B" to "C") and no unloading is applied. Simulations are therefore terminated after 2μs and the unloading behaviour is not captured.

The experimental and numerical results can be compared in Figure 5. The arrival time of the stress wave and the HEL are captured well, as are the peak plateau values for the first four impact velocities. However, the post-HEL behaviour shows a major mismatch between experiments and simulations. This mismatch will be investigated closer to find its origin.

3.2.1. Changing post-HEL behaviour

For plate impact tests the post-HEL behaviour is determined by the inelastic response of the ceramic material. When using a material model such as the JH2-V model this relates to the plastic deformation and softening of the material. The velocity profiles obtained from the simulations in Figure 5 indicate a rapid loss of material strength. The experiments show a smooth post-HEL behaviour, indicating that failure of the material is more gradual and strength is retained for a longer time. To introduce this effect in the JH2-V model the softening related parameter d_1 and the viscosity parameters η and λ_t are obvious choices. However, in the JH2-V model the material strengths (intact and residual) may also play a role. The intact strength can be directly obtained from experiments, thus is a known quantity. The residual strength of ceramics is less certain, hence its effect on the post-HEL behaviour will be considered, more specifically the effect of the B parameter from (6).

Figure 6 presents the velocity profiles for the spall test simulated with a larger residual strength. In the current results $B = 0.81$, while the previous results were obtained with $B = 0.31$. The current results show a closer agreement with the experiments. The post-HEL behaviour is now more smooth and also the peak plateau is reached at a time comparable to experiments. Although the post-HEL velocities are lower than the experimental values it can be found that increasing the B parameters improves the simulation results. It is however important to realize that there is almost

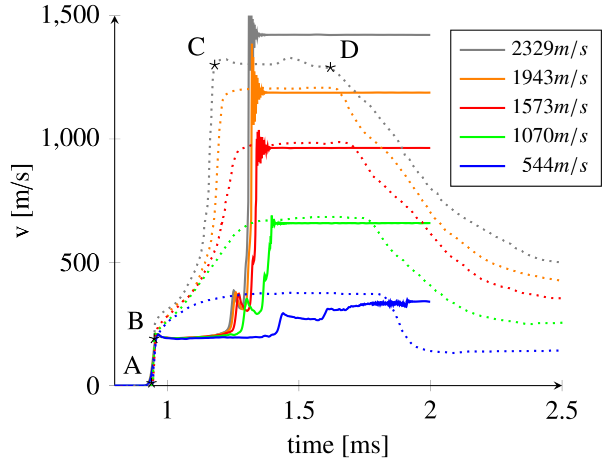

Figure 5: *Simulation results for a plate impact test on alumina ceramic. The JH2-V model with the parameter set for the spall test is used, with a slightly increased material stiffness, density, P_{HEL} and σ_{HEL}. There is clearly a large difference in post-HEL behaviour. The dotted lines show the experimental results from [54], the solid lines are simulation results.*

no loss in strength for the chosen value of residual strength, as $B = 0.81$ lies close to the intact strength parameter $A = 0.93$. It is known that a ceramic pulverizes under impact, which greatly reduces strength. So, although the plate impact results for simulations and experiments have a better match than before, it is not likely that this is a physically acceptable solution. There are other ways to retain a high material strength, such as a slower rate of damage.

The rate of damage in the JH2-V model is directly controlled by the failure strain formulation given in (9), as well as indirectly through the viscosity parameters η and $\dot{\lambda}_t$. The most obvious way of lowering the rate of damage is by increasing the d_1 parameter. Figure 7 shows the plate impact results for $d_1 = 0.050$, which is a factor ten larger than the $d_1 = 0.005$ used in the spall simulations. This higher value of d_1 makes the behaviour more ductile. For these results it is clear that the post-HEL gives a more smooth behaviour. The lowest two impact velocities seem to match well with the experimental results. However, for the highest three velocities the post-HEL curve is convexly shaped. Both the experimental results and the simulation with a higher B show a more concave response.

The convexly shaped simulation response of the highest three impact velocities indicate that the damage rate is now too slow for these cases. To speed up the rate of damage one can change the viscosity parameters. Since the viscosity η was already determined by the spall test, only the threshold rate $\dot{\lambda}_t$ can be altered. It is important to choose a threshold rate which leaves the lowest two velocities unaffected since they already show good agreement between simulations and experiments. After some parametric study a threshold value $\dot{\lambda}_t = 40 \cdot 10^3$ s^{-1} was selected. This value is higher than the maximum rate experienced in the 1070m/s test, but below the maximum experienced rate in the 1573m/s test. Figure 8 holds the results for the new threshold rate. This new threshold is found to improve the results as the higher impact velocity results now show a more concave response in the post-HEL behaviour. The current value of the threshold rate does not pose a problem for the spall simulations, as the threshold rate of $\dot{\lambda}_t = 40 \cdot 10^3$ s^{-1} is not reached during the spall simulations. Changing the threshold rate improves the simulation results. There is however still delay in the highest impact results compared to experiments, which can be found in the post-HEL behaviour as well as the peak plateau arrival time. Additional parametric study showed that the results can improve further by increasing the d_1 parameter once more to $d_1 = 0.500$. Results for this parameter set can be found in Figure 9. The parameter sets introduced in this section are also shown in Table 2 in the columns labeled 'variation 1, 2, 3'. Since none of these three parameter sets appears to be better than the other, a deeper investigation is required.

3.2.2. Plate impact concluded

When moving from spall simulations to plate impact simulations it was clear that the JH2-V model with a single set of material parameters was not able to properly predict both experiments. A major mismatch was found in the post-HEL behaviour of the material. The largest contributions were found to come from material softening, viscosity and the residual strength. Altering material properties resulted in a good match between experiments and simulations.

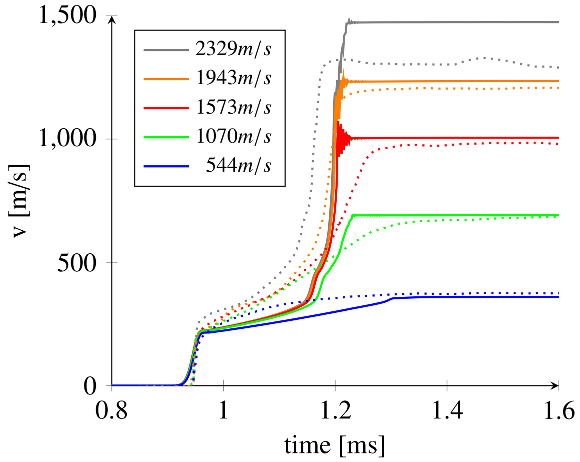

Figure 6: *Simulation results for a plate impact test on alumina ceramic. The parameter set used to obtain Figure 5 was also used here, but the residual strength parameter B is now increased to $B = 0.81$. The post-HEL behaviour is now more smooth and the peak plateau arrival time is now also closer to the experimental values. The dotted lines show the experimental results from [54], the solid lines are simulation results.*

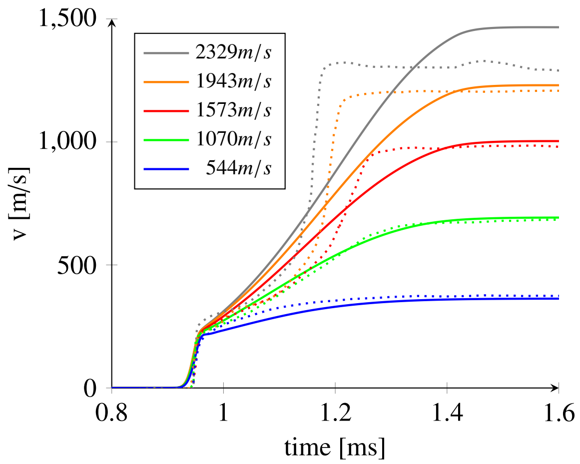

Figure 7: *Simulation results for a plate impact test on alumina ceramic. The parameter set used to obtain Figure 5 was also used here, but with a softening parameter $d_1 = 0.050$. The dotted lines show the experimental results from [54], the solid lines are simulation results.*

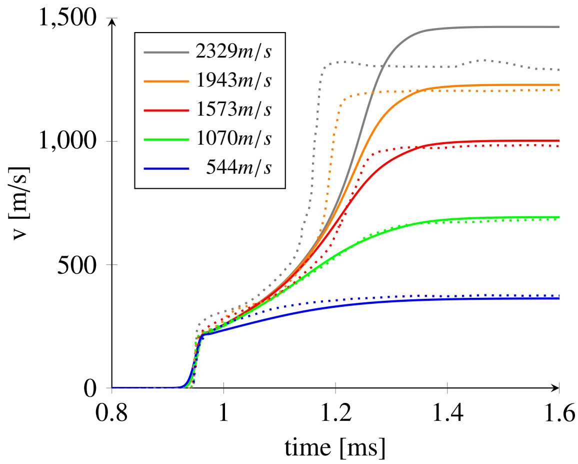

Figure 8: *Simulation results for a plate impact test on alumina ceramic. The parameter set used to obtain Figure 5 was also used here, but with* $d_1 = 0.050$ *and* $\dot{\lambda}_t = 40000s^{-1}$. *The dotted lines show the experimental results from [54], the solid lines are simulation results.*

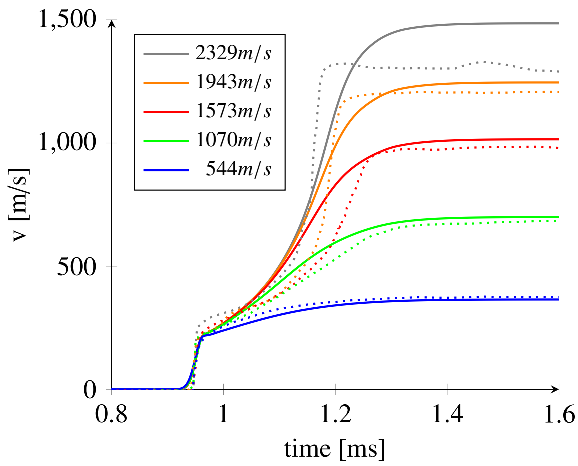

Figure 9: *Simulation results for a plate impact test on alumina ceramic. The parameter set used to obtain Figure 5 was also used here, but with* $d_1 = 0.500$ *and* $\dot{\lambda}_t = 40000s^{-1}$. *The dotted lines show the experimental results from [54], the solid lines are simulation results.*

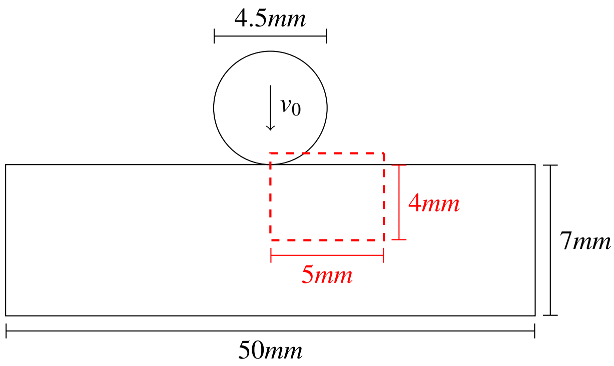

Figure 10: *Spherical impact test, the projectile is given an initial velocity v_0. Geometry of the simulated problem is given. The red dashed box is the spatial domain in which the simulation results will be presented. Note that the figure does not show the true aspect ratios.*

However the residual strength had to be increased by a factor three and the failure strain even by a factor ten or hundred. These changes can no longer be explained by small differences in the tested materials. Hence, these large variation in the model parameters indicate that there is an inconsistency in the formulation. The current results do however not show if the mismatch is caused by the softening/viscosity or the residual material strength. In the next subsections additional tests will be performed to further investigate the origin of this mismatch.

3.3. Spherical impact

Two types of impact tests have been simulated and analyzed so far. One in which failure occurred under tension (spall test) and one where failure occurred under compressive loading (plate impact). In both cases a dense alumina ceramic was used and an uniaxial deformation was imposed. These two extremes in loading condition did not give a unique answer in terms of material properties. In the current section a spherical impact test is simulated where the deformation is far from uniaxial and a wide range of stress states is encountered. Compression, tension and mixed mode loading will be found in this test, which can help revealing the correct material model behaviour.

In spherical impact experiments a projectile is given an initial velocity v_0 and impacts on a target material. This test is schematically shown in Figure 10. In the current section a steel projectile is assumed to impact on a ceramic target material. During this interaction both the projectile and target undergo (in)elastic deformation. Experimental results of spherical impact on alumina ceramic and silicon carbide ceramic are shown in Figures 11a, 11b and 11c. The figures show that the main mode of failure in the ceramic is cone cracking. The silicon carbide results also show a dark zone directly below the impact site. This is referred to as the quasi-plastic zone, which is characterized by micro-cracking and even plastic deformation. It is important to notice that the material in this subsurface zone is not pulverized. Although there is damage to the material the strength has not yet reduced to its minimum. This knowledge will prove vital in analyzing the spherical impact results.

The spherical impact experiment is simulated. The projectile is assumed to be a sphere with a diameter of 4.5mm, made of SAE51200 ball bearing steel. A Johnson-Cook material model was used to simulate this steel material, with a yield stress of 2.2GPa and hardening parameters from [58]. In the current simulations temperature and rate effects on the yield stress of the steel are ignored. The target is a ceramic plate with a thickness of 7mm and lateral dimension of 50mm (see Figure 10). The ceramic plate is not supported and without any material attached to the back surface. The ceramic material itself is a high density alumina ceramic, similar to the material previously considered in the spall and plate impact experiments. For the ceramic material the JH2-V model is used. As base model parameters the values from the plate impact test are chosen, as well as the three variations introduced in the previous section. These parameter sets can be found in Table 2 in the columns 'Plate impact' and 'variation 1,2,3'. The variations correspond to the parameter sets used to obtain the plate impact results from Figures 6, 8 and 9. The sphere impact experiment is simulated in a 2d axi-symmetric formulation, with the axis of impact as obvious axis of symmetry. Any lateral movement is constrained along this axis of symmetry and no other boundary conditions are applied to the system. As such the ceramic can be considered a free standing or unsupported target. Three noded linear elements are used to

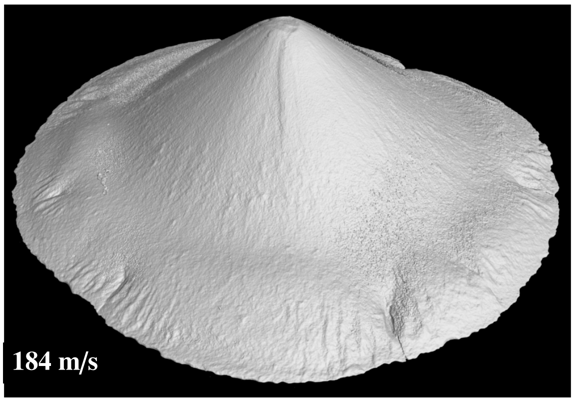

(a) *An alumina ceramic cone, retrieved after a spherical impact experiment (E.P. Carton, TNO, personal communication, 2018). Figure was obtained by X-ray imaging (A. Thijssen, Delft University of Technology, personal communication, 2018).*

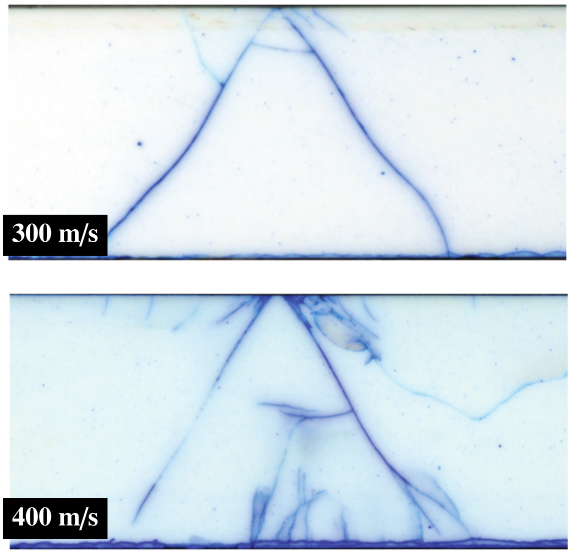

(b) *Alumina ceramic after spherical impact, pictures are obtained from [56]. Comminution of ceramic directly below the projectile is absent.*

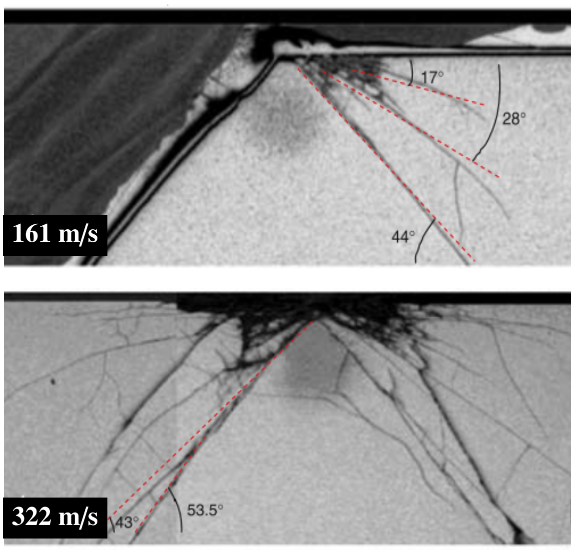

(c) *Silicon carbide ceramic after spherical impact, pictures are obtained from [57]. A quasi-plastic zone is found below the projectile, but the material is not comminuted.*

Figure 11: *Experimental results for a steel sphere impacting ceramic tiles. Top figure shows the result of impact on a ceramic plate without backing, the bottom figures are cross-sections of ceramic plates with backing after impact. Projectile velocities are shown. Cone cracking is clearly visible in all cases.*

mesh this problem. The mesh is unstructured and the element size ranges from $h \approx 0.05$mm along the axis of impact to $h \approx 1.0$mm at the far side of the ceramic target. A penalty stiffness model with Coulomb friction ($\mu = 0.5$) is used to describe the contact between projectile and target.

Figure 12 shows the ceramic damage after spherical impact using four different parameter sets for the JH2-V model. The figures show only the material directly underneath the projectile corresponding to the dashed box shown in Figure 10. For all cases the alumina ceramic is impacted by a steel sphere with an initial velocity of 200m/s. The figures are taken after 1.4μs of simulated time. For the given tile thickness and elastic properties this is sufficient time for the initial pressure wave to travel to the back surface of the ceramic tile and return to the impact surface. This time is long enough to study the initiation of failure, but not enough to observe if the projectile is stopped by the ceramic. Although the latter is interesting from a practical point of view, the former is sufficient to investigate the previously found mismatch in parameters.

All cases show cone cracking (see Figure 12). However, the reference set and variation 1 of the model parameters both show a zone of fully failed material ($D = 1.0$) directly underneath the projectile. From (2) it can be found that these zones retain a strength under compression, but can no longer sustain any tensile loading. This is typical behaviour of fragmented material, which is what a ceramic is expected to be after full failure under compressive loading. Recall that full fragmentation was not observed in experiments (Figure 11), where some damage could be found underneath the projectile but the ceramic was not pulverized. This shows that the parameter set with a fast softening and the set with a high residual strength can not be correct. The variations 2 and 3, which have a slower softening than the reference set, provide a better match with experiments. Variation 2, with $d_1 = 0.050$, shows a cone crack as well as a (semi-) spherical zone of damage below the projectile. Although this is an improvement from the fully failed top layer found for a fast softening these results would still indicate a fully comminuted material. The best match with experiments is found for variation 3 with $d_1 = 0.500$, for which a clear cone crack forms. For this case minor damage is predicted below the projectile ($D \approx 0.01$), but the material is not fully failed as in the other cases. This minor damage is found from the figure as an ever so slightly light blue discolouration.

3.3.1. Spherical impact concluded

The plate impact and spall test have shown that it was impossible for the JH2-V model with a single parameter set to match both sets of experimental results. It was argued that both softening/viscosity or residual strength could be the reason for this mismatch. However, the spall and plate impact tests did not offer any certainty as to which option was the correct one.

Spherical impact was proposed as a third test case. This experiment is often performed on armour ceramics, where the main failure mechanism is cone cracking as well as some (incomplete) subsurface damage. Spherical impact simulations showed that these mechanisms could only be predicted for material with a slow softening and not for material with a high residual strength. So the spherical impact test has shown that the mismatch in earlier simulations and experiments was caused by the softening and viscosity.

For the plate impact experiment it was shown that slow softening is required. In the spall test a fast softening was assumed. However, it also would have been possible to use slow softening for the spall test and tune the viscosity accordingly. So, although the previous experiments have shown that there is some mismatch between experiments and simulations, the mismatch can still be solved by recalibration of the parameters. In the next section one more experiment is considered to investigate this behaviour.

3.4. Ring on ring

Three types of tests have been performed so far, namely a spall test with pure tensile loading, a plate impact test with pure compressive loading and a spherical impact test where a wide range of stress states including both tensile and compressive stresses. The results for these tests have shown an inconsistency in the material softening modeling. For the spall test a softening parameter $d_1 = 0.005$ was used, for which the material softening is fast and the response may be considered as being brittle. However, plate and spherical impact showed good agreement with simulations using $d_1 = 0.500$, for which the softening is slow and the response is more ductile. A possible solution to this inconsistency would be to increase the softening parameter for the spall test. In fact, the spall experiments could also be matched for $d_1 = 0.500$ by tuning the viscosity parameters. However, increasing d_1 would jeopardize the brittle response of ceramics under tension. This would be highly unwanted since the brittle nature of (armour) ceramic under tensile loading is a well accepted material trait.

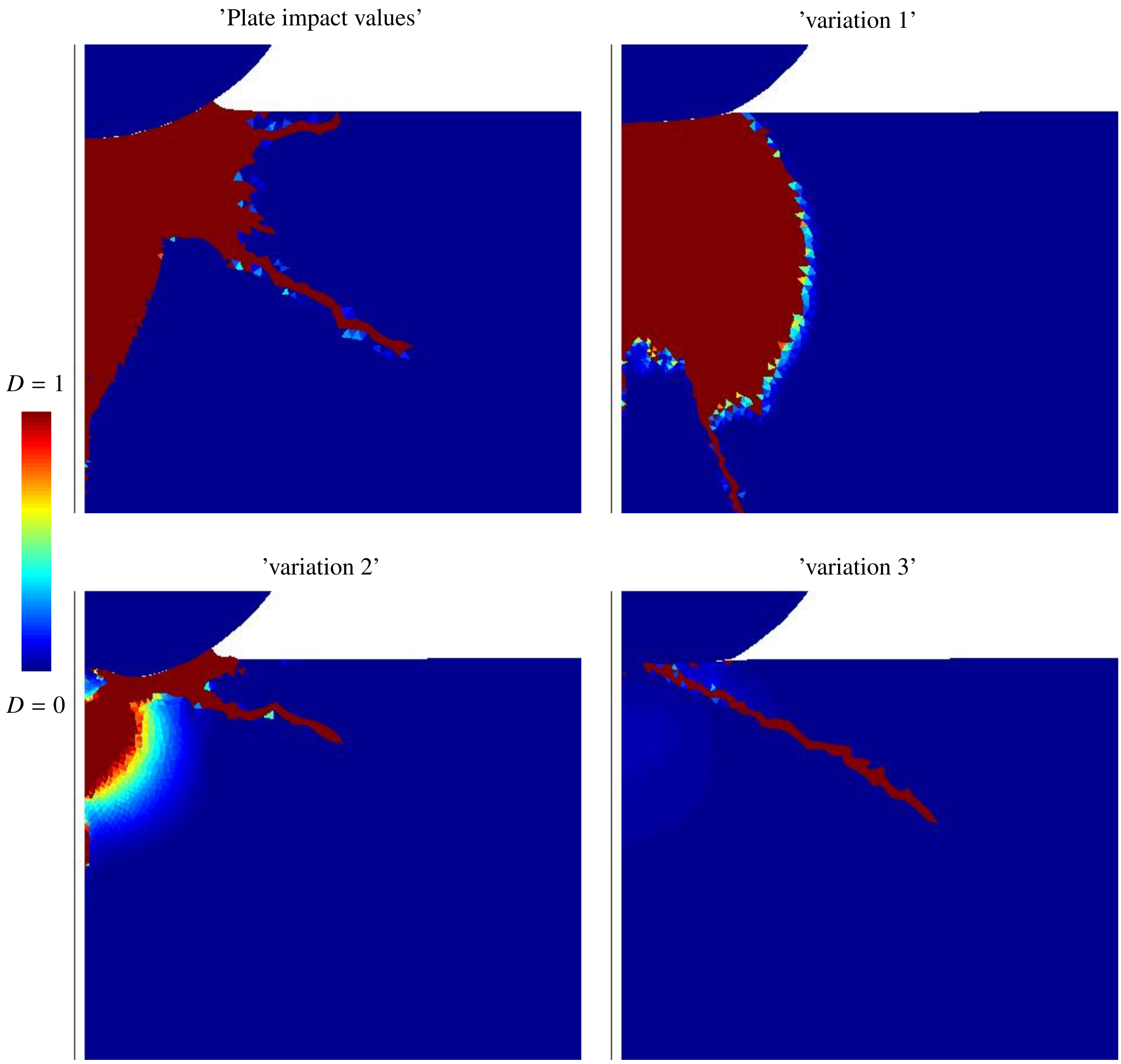

Figure 12: *Spherical impact results for the JH2-V model. Damage variable $D \in [0..1]$ is shown after $1.4\mu s$ of simulated time.*

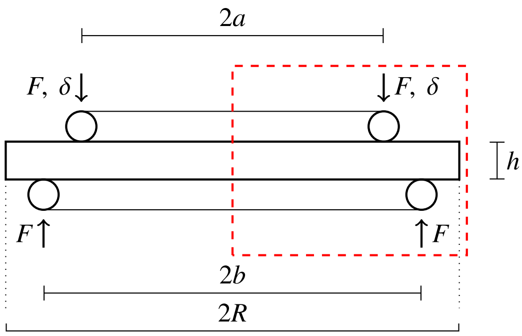

Figure 13: *Ring on ring bending experiment. The red dashed box is the spatial domain which is used for a 2D axisymmetric simulation of the experiment.*

A ring-on-ring (ROR) bending test is considered as final test. This is a tensile dominated test, where a disk of material is supported by a large ring on the bottom and loaded through a smaller ring on top. This creates a constant and bi-axial bending moment in the specimen inside the smaller ring. Figure 13 gives a schematic representation of the ring-on-ring test. The test is controlled by applying a deformation δ on the smaller inner ring, a force can then be measured either in the same ring or on the large bottom ring. The test is performed at a very slow loading rate ($\dot{\delta} = 0.1mm/s$), such that the test can be considered quasi-static and inertia effects can be excluded. The low loading rate removes the dynamic effects such as wave propagation and allows to focus solely on the material failure. Please note that the material rate dependency from the JH2-V model is still present, even though inertial effects are excluded by using quasi-static simulations. The only requirement is that there is some measure of (pseudo) time in the simulation, which can be found from the applied deformation rate $\dot{\delta} = 0.1mm/s$. This ensures the material model retains its regularizing properties.

An analytical solution for the stress field inside the specimen under ROR loading exists [59, 60]. This makes it possible to relate an applied force to a (tensile) stress in the disk and find the strength of the tested material. The tensile stresses in radial (σ_r) and tangential direction (σ_θ) at the bottom of the specimen, inside the internal ring can be given as

$$\sigma_r = \sigma_\theta = \frac{3F}{4\pi h^2}\left[2(1+\nu)\ln\left(\frac{a}{b}\right) + \frac{(1-\nu)(a^2-b^2)}{R^2}\right], \tag{11}$$

where F is the applied force, ν the Poisson's ratio, h the specimen thickness and a, b, R the radii of the internal ring, external ring and specimen.

Experimental results for ROR bending on alumina ceramics are available in literature. In [61] an ultimate tensile stress of Wesgo alumina is presented ranging from 190 to 260MPa. In [26] the experimental results show the ultimate tensile stress ranges from $168.6-232.7$MPa. Between these two sources the experimental set-up differs in dimensions and the alumina ceramics are similar but not exactly the same.

The geometry of the test as presented in [26] was assumed, such that $R = 9$mm, $a = 5$mm, $b = 8$mm and $e = 1$mm. Since the ROR experiment was performed on the same material as the spall test the model parameters for spall are used as (brittle) base values. A more ductile behaviour is found by using $d_1 = 0.500$. The parameter sets used in the ROR simulations are those found in columns 'Spall' and 'variation 4' from Table 2. The ROR problem is simulated in a 2d axi-symmetric strain formulation. Here the center of the disk is considered as axis of symmetry, where all horizontal movement is constrained. Vertical movement is constrained for a single node on the bottom of the disk, at distance b. Vertical displacements are imposed on a single node on the top surface of the disk, at distance a. The mesh for this problem is unstructured and three noded linear triangular elements are used with a size $h \approx 0.025$mm. Figure 14 holds the force and displacement measured on the inner top ring during the simulation. The figure also shows two hatched zones corresponding to the experimental results from [61] and [26], for which the reported failure stresses were converted to forces using (11). When comparing to the experimental results it is clear that slow softening results in an overestimated material strength, while an acceptable material strength is found with fast softening of the material. The maximum stress found in the simulations was 240MPa and 329MPa for the fast and slow softening cases respectively.

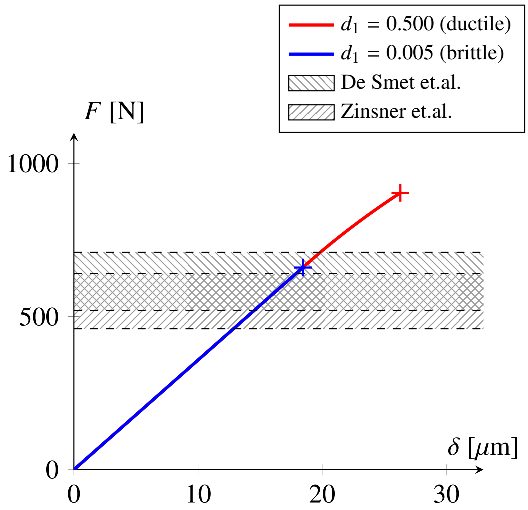

Figure 14: *Ring on ring bending test. Results are obtained by simulation with the JH2-V material model, for two values of softening. The simulations fail to converge at the crosses, this is when a large number of points fail under apex return. This may be seen as the sudden and brittle failure of the specimen. The ultimate force for the two tests is found as* 662*N and* 904*N, corresponding to tensile stresses of* 240*MPa and* 329*MPa. Experimentally measured ranges from De Smet [61] and Zinsner [26] are given by the hatched areas.*

3.4.1. Ring-on-Ring concluded

The ring-on-ring test confirms that a fast softening is required under tension. Earlier it was demonstrated that slow softening was required for the compression dominated tests. This shows the obvious need for a separation in material softening, where controlling the response under tension and compression independently is possible. The next section will show that a separated material softening can indeed be used to match all previously described experiments, with a single set of parameters.

4. JH2-V model improvement

The experiments and simulations in the previous sections have shown that the original failure strain formulation of the JH models is inadequate. The analyzed experiments could only be matched by changing softening related parameters and could not be captured by a single set of model parameters.

For a ceramic the failure mechanisms under compression and under tension are significantly different. Failure under tension occurs by brittle fracture of the material, while a ductile response can be found under sufficiently high compression. Under high compression failure is characterized by crystal plasticity and micro-cracking. If the failure mechanisms under tension and compression are so different, it is reasonable to also distinguish between these two mechanisms in the material model. The material models by Deshpande-Evans and Simha presented in the section 2 acknowledge that a ceramic material has multiple failure mechanisms. These models capture each of the different failure mechanisms by its own softening/damage behaviour. In the JH2 material model failure is captured by the failure strain formulation (9). This single formulation includes a pressure dependency, but does not offer a clear separation in behaviour for each of the failure mechanisms. In fact the function couples the behaviour under tension and compression through the softening parameters d_1 and d_2. Because of this coupling, changing the failure strain under compression will inadvertently change the damage rate under tension and vice versa. In a recent publication the limited flexibility of the JH failure strain formulation (9) was also addressed [62], albeit for glass material using different strength formulations. In the publication a shift was proposed to the failure strain, to have zero plastic deformation to failure under low pressures and allow for accumulation of plasticity beyond some pressure threshold. This does indeed provide a clear separation between brittle tensile failure and more ductile compression failure. Such approach can however not be used in the current visco-plastic framework, since a non-zero plastic strain is required to activate viscosity and obtain regularization.

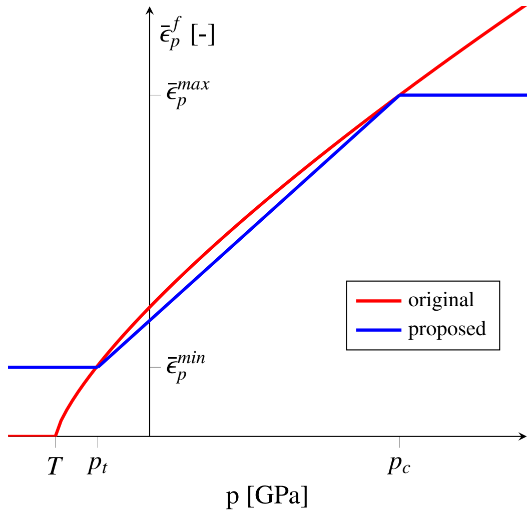

Figure 15: *Failure strain as function of pressure, in the original JH2 and the proposed formulation.*

A new softening formulation is proposed, in which the damage rate under tension and compression can be controlled independently. The formulation for the rate of damage can remain the same as (8). The failure strain formulation from (9) is replaced by the tri-linear equivalent plastic strain formulation

$$\bar{\epsilon}_p^f(\boldsymbol{\sigma}) = \begin{cases} \bar{\epsilon}_p^{min}, & p(\boldsymbol{\sigma}) < p_t \\ \left(\bar{\epsilon}_p^{max} - \bar{\epsilon}_p^{min}\right)\left(\frac{p(\boldsymbol{\sigma})-p_t}{p_c-p_t}\right) + \bar{\epsilon}_p^{min}, & p_t < p(\boldsymbol{\sigma}) < p_c \\ \bar{\epsilon}_p^{max}, & p_c < p(\boldsymbol{\sigma}). \end{cases} \tag{12}$$

This formulation assumes a failure strain $\bar{\epsilon}_p^{min}$ for pressures below p_t, a failure strain $\bar{\epsilon}_p^{max}$ for pressures above p_c and interpolates between these two values for intermediate pressures. This formulation allows for independent changes to the failure strain and thus damage rate under tension and compression. Furthermore, the model is simple, providing a clear advantage when calibrating the model as will be shown later in this section.

The proposed failure strain formulation is shown together with the original failure strain formulation in Figure 15. In this figure the failure strain is plotted for arbitrary model parameters. The proposed model parameters can be chosen such that the original formulation is linearly approximated in the domain $p_t < p < p_c$, but obviously this is not required.

The new formulation (12) requires information on the failure strains, as well as a pressure range for which the behaviour transitions from brittle to ductile. For brittle materials it is not uncommon to have a transition from brittle to ductile behaviour. Often this is linked to an ambient temperature, but a transition can also be found at a given confining pressure [63, 64, 65]. To use the proposed formulation one should ideally know the transition pressure. If this data is not available one may calibrate the model for a given test under tension and one under compression. The latter approach will be used in this paper.

The spall and plate impact tests from the previous section can be used to calibrate the newly proposed failure strain formulation. These tests provide insight in the failure behaviour under uniaxial tensile and compressive loading. Results from sections 3.1 and 3.2 showed that the failure strain might differ by a few orders of magnitude between uniaxial tensile or compressive loading. A first approximation of the model parameters in equation (12) can be obtained as follows.

First consider uniaxial tensile loading on a ceramic with the material properties from Table 2. Under these conditions the yield strength will be reached at a pressure $p_{min} = -0.17$GPa. In the original failure strain formulation with $d_1 = 0.005$ this pressure leads to $\bar{\epsilon}_p^f(p_{min}) = 0.00015$. Similarly for uniaxial compressive loading a pressure of $p_{max} = 3.02$GPa is found and $d_1 = 0.500$ leads to a failure strain of $\bar{\epsilon}_p^f(p_{max}) = 0.4965$. Here the original model parameter d_1 was chosen as the values for which spall and plate impact simulations agreed well with experimental

Table 3: *JH2-V model parameters using the improved failure strain formulation from* (12). *The model parameter sets for each test are shown. Only the stiffness, density and Hugoniot pressure are changed, which is justified because of small differences in experimentally tested ceramics.*

variable	unit	Spall value	Plate impact value	Sphere impact value	ROR value
E	GPa	360.0	**380.0**	**380.0**	360.0
ν	-	0.22	0.22	0.22	0.22
ρ	kg/m^3	3850	**3890**	**3890**	3850
A	GPa	0.930	0.930	0.930	0.930
B	GPa	0.310	0.310	0.310	0.310
n	-	0.6	0.6	0.6	0.6
m	-	0.6	0.6	0.6	0.6
C	-	0.0	0.0	0.0	0.0
T	GPa	0.2	0.2	0.2	0.2
η	GPa·s	$0.028{\cdot}10^{-3}$	$0.028{\cdot}10^{-3}$	$0.028{\cdot}10^{-3}$	$0.028{\cdot}10^{-3}$
$\dot{\lambda}_t$	s^{-1}	$4 \cdot 10^4$	$4 \cdot 10^4$	$4 \cdot 10^4$	$4 \cdot 10^4$
HEL	GPa	6.25	6.25	6.25	6.25
P_{HEL}	GPa	3.50	**3.25**	**3.25**	3.50
σ_{HEL}	GPa	4.125	**4.50**	**4.50**	4.125
$\bar{\epsilon}_p^{min}$	-	$1.5 \cdot 10^{-4}$	$1.5 \cdot 10^{-4}$	$1.5 \cdot 10^{-4}$	$1.5 \cdot 10^{-4}$
$\bar{\epsilon}_p^{max}$	-	0.4965	0.4965	0.4965	0.4965
p_t	GPa	-0.17	-0.17	-0.17	-0.17
p_c	GPa	3.02	3.02	3.02	3.02

results. This procedure is also visualized in Figure 16, where the top graphs shows the intact material strength with uni-axial loading directions and the bottom graph shows the failure strain. For the failure strain the original and proposed formulations are plotted. This procedure shows how simple it is to calibrate the proposed failure strain model, using just two well established experiments.

The newly proposed tri-linear failure strain formulation (12) will now be used to simulate spall, plate impact, spherical impact and the ring-on-ring test. If the formulation is an improvement over the original one, all four experiments should be matched by the simulations. The JH2-V model parameters used in this final section of the paper, for the various tests, are shown in Table 3. The model parameters related to viscosity and failure are kept the same in all simulations. The only variations in parameters are those in stiffness, density and Hugoniot pressure. These are well justified since the experimentally tested materials showed small variations in the elastic properties, as discussed in section 3.1.

Figure 17 provides the predicted spall strength as a function of loading rate, when using the proposed tri-linear failure strain formulation. The rate dependency in the spall strength is still captured by the model. The strengths of the JH2-V model with original and the proposed softening formulation are a very close match. This can be easily explained, as the problem is tension dominated and both formulations used a minimal failure strain $\bar{\epsilon}_p^{min} = 0.00015$ (see (10) and (12)). When the failure zone of the simulation is compared to the experiment in Figure 18, it is found that the failure zones agree well.

Figure 19 shows the inter-facial velocities measured in the plate impact simulation using the tri-linear failure strain formulation. The results agree well with the experimental results and are quite similar to those obtained with the original JH2 formulation with $d_1 = 0.500$. Again this can be easily explained since the problem is compression dominated and the failure strain in the original or tri-linear formulation is of the same order.

Figure 20 shows the damage predicted by a spherical impact simulation using the tri-linear failure strain formulation. The results are similar to those for $d_1 = 0.500$ from Figure 12. That is, a cone crack is predicted and some minor subsurface damage is present. Two differences can be found when comparing to the results from Figure 12. The first is that the cone crack for the tri-linear failure strain extends further into the target material. This can be explained by the more brittle behaviour found at tensile states in the new formulation. The second difference is that the tri-linear

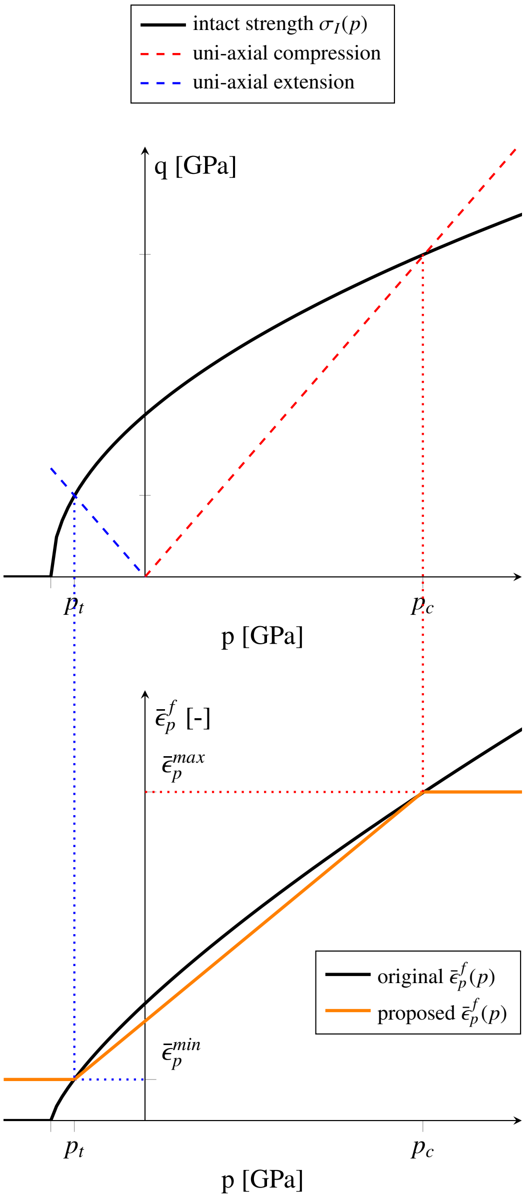

Figure 16: *Intact material strength and failure strains plotted as a function of pressure. The original and proposed tri-linear failure strain is shown. The proposed failure strain formulation is fitted to the original failure strains, found under uni-axial deformation of the ceramic.*

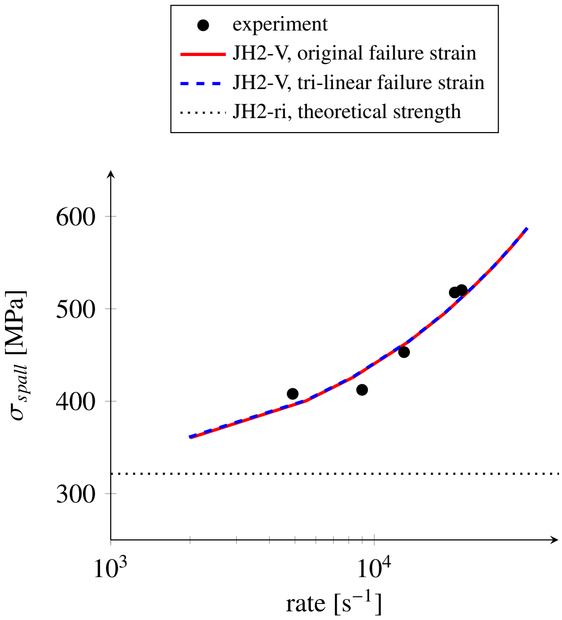

Figure 17: *Spall strength, experimentally measured and predicted by simulation. The proposed tri-linear failure strain model is used, all cases use $\eta = 0.028 \cdot 10^{-3}$ GPa·s and $\lambda_t = 40 \cdot 10^3\ s^{-1}$ as these values were used to obtain good results in spherical impact simulations. A minimal failure strain $\bar{\varepsilon}_p^{min} = 1.5 \cdot 10^{-4}$ is used for both the original and the tri-linear failure strains.*

formulation results show more damage at the target surface. Again this is a zone where the pressure is low (or even negative), for which the behaviour is brittle in the tri-linear formulation.

As a final step the ring-on-ring simulations are performed with the newly proposed failure strain formulation. A tensile strength is found of 251MPa. This is slightly higher than the previously found value for the original model with $d_1 = 0.005$. However, the strength predicted by the newly proposed model still falls withing the experimentally measured ranges (190 – 260MPa from [61] and 168.6 – 232.7MPa from [26]).

5. Conclusions

A ceramic material may fail as a consequence of different mechanisms. Depending on the stress state in the material one or more of these failure mechanisms may be activated. Since the mechanisms are different, so should the modeling of these mechanisms be. The original JH2 model does not distinguish between different failure mechanisms. In the JH2 model the rate of damage is determined by the failure strain. This failure strain is a function of pressure, where tensile states have a low strain to failure and a brittle response while high pressures have a high strain to failure and a more ductile response. The failure strain is, however, a single function and behaviour under tension and compression are inseparably coupled. By simulating a number of experiments under different loading conditions it was shown that this single function is indeed incapable of properly capturing the behaviour of the various failure modes in ceramic material.

Four experiments were simulated using the JH2-V model with the original JH2 failure strain formulation. All experimental results were obtained from literature and in all experiments a similar high purity alumina ceramic was considered. The first experiment was spall, which loads the material in uni-axial extension. The second experiment was plate impact, loading the material in uni-axial contraction. Spherical impact was the third experiment, in which the material experiences a wide range of stress states. As a final test ring-on-ring bending was considered, a quasi-static test with failure of the material in bi-axial tension.

Simulation of spall and plate impact experiments showed that a match for both could only be obtained by changing the material parameters. Either increasing the residual strength of the material or the failure strain of the material was required to match the plate impact experiments by simulation. A recalibration of the model parameters would

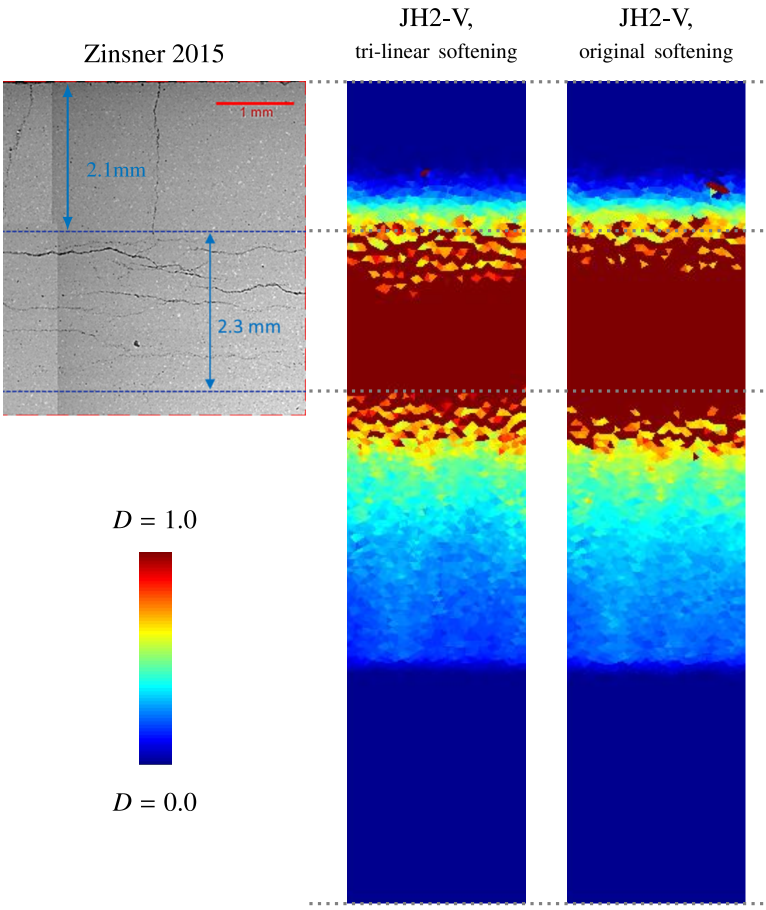

Figure 18: *Damage profiles obtained in the spall experiment [26] and FE simulations. Stress wave 2 from Figure 2a is applied. The JH2-V material model with original and newly proposed tri-linear failure strain formulation is compared.*

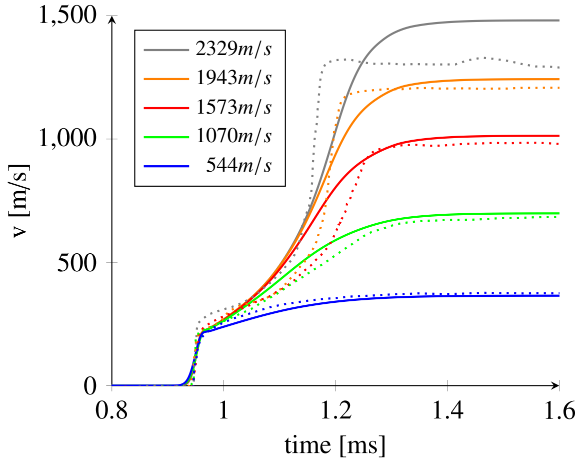

Figure 19: *Simulation results for a plate impact test on alumina ceramic. The parameter set for the spall test is used, but with the newly proposed failure strain formulation and* $\dot{\lambda}_t = 40000s^{-1}$*. The results are very similar to those obtained with the original JH2 formulation with* $d_1 = 0.500$ *and* $\dot{\lambda}_t = 40000s^{-1}$*, from Figure9. The dotted lines show the experimental results from [54], the solid lines are simulation results.*

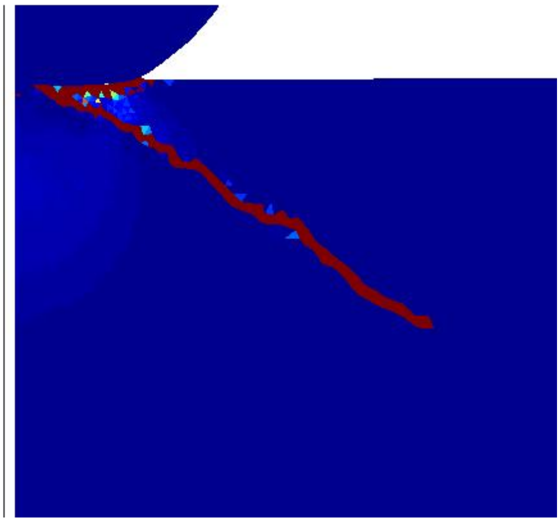

Figure 20: *Spherical impact results for the JH2-V model with tri-linear failure strain. Cone cracks are clearly visible, as well as some minor subsurface damage. Complete failure of the ceramic below the projectile is not observed.*

be sufficient to match both types of tests, although this would increase some model parameters by a few orders of magnitude compared to what is used in literature.

The spherical impact experiments and simulations were used to investigate the parameter choice in the material model. Increasing the residual strength of the material, which was found to give a match in plate impact results, did not lead to good results in the spherical impact test. It was found that a match with experiments could only be found by increasing the failure strain. At this point recalibrating the failure strain parameters would be sufficient to find matching results of the spall, plate impact and spherical impact tests. However, doing so would require a failure strain two orders of magnitude larger than what was reported in literature. This could jeopardize the brittle behaviour of the material under tension.

As a final check a ring-on-ring test was simulated. This quasi-static test loads the material in bi-axial tension. It was shown that the material tensile strength was greatly overestimated when using a high failure strain.

The results of the four experiments and simulations showed that the ceramic material required both a high and a low failure strain, depending on the stress state. The original failure strain formulation in the JH models could not be tuned to provide this range of failure strains. A new tri-linear formulation was proposed, in which failure strains under tension and compression were treated as independent quantities. With this formulation a brittle response could be obtained under tension, while maintaining a ductile response under compression. It was shown that this new formulation could be used to match all experiments considered in the paper, for a single set of failure parameters. The latter is key, as this was not possible with the original failure strain formulation.

References

[1] P. J. Hazell, Ceramic Armour: Design and Defeat Mechanisms, Argos Press, Canberra, 2006.

[2] S. M. Walley, Historical review of high strain rate and shock properties of ceramics relevant to their application in armour, Advances in Applied Ceramics 109 (8) (2010) 446–466. `doi:10.1179/174367609X422180`.
URL `http://www.maneyonline.com/doi/abs/10.1179/174367609X422180`

[3] Z. Rosenberg, E. Dekel, Terminal ballistics, 2nd Edition, Springer-Verlag, Heidelberg, 2012.

[4] J. Cagnoux, F. Longy, Spallation and shock-wave behaviour of some ceramics, Le Journal de Physique Colloques 49 (C3) (1988) C3–3–C3–10. `doi:10.1051/jphyscol:1988301`.
URL `http://www.edpsciences.org/10.1051/jphyscol:1988301`

[5] J. Lankford, C. E. A. Jr, A. J. Nagy, J. D. Walker, A. E. Nicholls, Inelastic response of confined aluminium oxide under dynamic loading conditions, Journal of Materials Science 33 (1998) 1619–1625.
URL `http://link.springer.com/article/10.1023/A:1017576123026`

[6] S. Acharya, S. Bysakh, V. Parameswaran, A. Kumar Mukhopadhyay, Deformation and failure of alumina under high strain rate compressive loading, Ceramics International 41 (5) (2015) 6793–6801. doi:10.1016/j.ceramint.2015.01.126.
URL http://dx.doi.org/10.1016/j.ceramint.2015.01.126

[7] J. Wade, S. Robertson, H. Wu, Plastic deformation of polycrystalline alumina introduced by scaled-down drop-weight impacts, Materials Letters 175 (2016) 143–147. doi:10.1016/j.matlet.2016.04.023.
URL http://dx.doi.org/10.1016/j.matlet.2016.04.023

[8] M. Bhattacharya, S. Dalui, N. Dey, S. Bysakh, J. Ghosh, A. Kumar Mukhopadhyay, Low strain rate compressive failure mechanism of coarse grain alumina, Ceramics International 42 (8) (2016) 9875–9886. doi:10.1016/j.ceramint.2016.03.087.
URL http://linkinghub.elsevier.com/retrieve/pii/S0272884216302231

[9] A. C. Fischer-Cripps, B. R. Lawn, Stress Analysis of Contact Deformation in Quasi-Plastic Ceramics, Journal of the American Ceramic Society 79 (10) (1996) 2609–2618. doi:10.1111/j.1151-2916.1996.tb09023.x.

[10] A. A. Wereszczak, T. P. Kirkland, K. T. Strong, T. J. Holmquist, Ornl quasi-static mechanical characterization and analysis : Fy09 annual report to tardec under contract de-ac05-00or22725, Tech. rep., Oak Ridge National Laboratory (2009).

[11] T. J. Ahrens, Material Strength Effect in the Shock Compression of Alumina, Journal of Applied Physics 39 (10) (1968) 4610. doi:10.1063/1.1655810.
URL http://scitation.aip.org/content/aip/journal/jap/39/10/10.1063/1.1655810

[12] W. H. Gust, E. B. Royce, Dynamic Yield Strengths of B4C, BeO, and Al2O3 Ceramics, Journal of Applied Physics 42 (1) (1971) 276. doi:10.1063/1.1659584.

[13] A. M. Rajendran, J. L. Kroupa, Impact damage model for ceramic materials, Journal of Applied Physics 66 (8) (1989) 3560–3565. doi:10.1063/1.344085.

[14] A. M. Rajendran, High Strain Rate Behavior of Metals Ceramics, and Concrete, Tech. rep., University of Dayton Research Institute, Dayton, Ohio (1992).
URL http://oai.dtic.mil/oai/oai?verb=getRecord&metadataPrefix=html&identifier=ADA252979

[15] Y. Partom, Calibrating a material model for AD995 alumina from plate impact VISAR profile, Journal de Physique IV 4 (C8) (1994) 495–500.

[16] D. E. Grady, R. L. Moody, Shock Compression Profiles in Ceramics, Tech. Rep. March, Sandia National Laboratories, Albuquerque (1996).

[17] D. E. Grady, Shock-wave compression of brittle solids, Mechanics of Materials 29 (1998) 181–203. doi:10.1016/S0167-6636(98)00015-5.

[18] T. J. Vogler, W. D. Reinhart, L. C. Chhabildas, Dynamic behavior of boron carbide, Journal of Applied Physics 95 (8) (2004) 4173–4183. doi:10.1063/1.1686902.

[19] E. B. Zaretsky, High temperature impact response of 998 alumina, Journal of Applied Physics 114 (18) (2013) 183518. doi:10.1063/1.4830014.
URL http://scitation.aip.org/content/aip/journal/jap/114/18/10.1063/1.4830014

[20] I. Girlitsky, E. Zaretsky, S. Kalabukhov, M. P. Dariel, N. Frage, Dynamic compressive and tensile strengths of spark plasma sintered alumina, Journal of Applied Physics 115 (24) (2014) 243505. doi:10.1063/1.4885436.
URL http://scitation.aip.org/content/aip/journal/jap/115/24/10.1063/1.4885436

[21] F. Gálvez, J. Rodríguez, V. Sánchez, Tensile strength measurements of ceramic materials at high rates of strain, Journal of physics IV France 7 (1997) 151–155.
URL http://jp4.journaldephysique.org/articles/jp4/abs/1997/03/jp4199707C328/jp4199707C328.html

[22] F. Gálvez, J. Rodríguez, V. Sánchez Galvez, Influence of the Strain Rate on the Tensile Strength in Aluminas of Different Purity, Journal of Physics IV 10 (2000) 323–328.

[23] F. G. Díaz-Rubio, J. R. Pérez, V. S. Gálvez, The spalling of long bars as a reliable method of measuring the dynamic tensile strength of ceramics, International Journal of Impact Engineering 27 (2002) 161–177.
URL http://www.sciencedirect.com/science/article/pii/S0734743X01000392

[24] J. Buchar, S. Rolc, Dynamic fracture of ceramics, Journal de Physique IV (Proceedings) 134 (2006) 681–686. doi:10.1051/jp4:2006134105.

[25] B. Erzar, E. Buzaud, Shockless spalling damage of alumina ceramic, European Physical Journal: Special Topics 206 (1) (2012) 71–77. doi:10.1140/epjst/e2012-01588-0.

[26] J.-L. Zinszner, B. Erzar, P. Forquin, E. Buzaud, Dynamic fragmentation of an alumina ceramic subjected to shockless spalling: An experimental and numerical study, Journal of the Mechanics and Physics of Solids 85 (2015) 112–127. doi:10.1016/j.jmps.2015.08.014.
URL http://dx.doi.org/10.1016/j.jmps.2015.08.014

[27] J.-L. Zinszner, B. Erzar, P. Forquin, Strain rate sensitivity of the tensile strength of two silicon carbides: experimental evidence and micromechanical modelling, Philosophical Transactions of the Royal Society of London A: Mathematical, Physical and Engineering Sciences 375 (2085). arXiv:http://rsta.royalsocietypublishing.org/content/375/2085/20160167.full.pdf, doi:10.1098/rsta.2016.0167.
URL http://rsta.royalsocietypublishing.org/content/375/2085/20160167

[28] G. R. Johnson, T. J. Holmquist, A computational constitutive model for brittle materials subjected to large strains, high strain rates, and high pressures, Shock Wave and High-Strain-Rate Phenomena in Materials.

[29] G. R. Johnson, T. J. Holmquist, An improved computational constitutive model for brittle materials, AIP Conference Proceedings 309 (1994) 981–984. doi:10.1063/1.46199.
URL http://scitation.aip.org/content/aip/proceeding/aipcp/10.1063/1.46199

[30] G. R. Johnson, T. J. Holmquist, S. R. Beissel, Response of aluminum nitride (including a phase change) to large strains, high strain rates, and high pressures, Journal of Applied Physics 94 (3) (2003) 1639. doi:10.1063/1.1589177.
URL http://scitation.aip.org/content/aip/journal/jap/94/3/10.1063/1.1589177

[31] C. Simha, S. J. Bless, A. Bedford, Computational modeling of the penetration response of a high-purity ceramic, International journal of impact engineering 27 (2002) 65–86.

URL http://www.sciencedirect.com/science/article/pii/S0734743X01000367

[32] V. S. Deshpande, A. G. Evans, Inelastic deformation and energy dissipation in ceramics: A mechanism-based constitutive model, Journal of the Mechanics and Physics of Solids 56 (10) (2008) 3077–3100. doi:10.1016/j.jmps.2008.05.002.
URL http://linkinghub.elsevier.com/retrieve/pii/S0022509608000975

[33] V. S. Deshpande, E. A. N. Gamble, B. G. Compton, R. M. McMeeking, A. G. Evans, F. W. Zok, A Constitutive Description of the Inelastic Response of Ceramics, Journal of the American Ceramic Society 94 (2011) s204–s214. doi:10.1111/j.1551-2916.2011.04516.x.
URL http://doi.wiley.com/10.1111/j.1551-2916.2011.04516.x

[34] E. C. Simons, J. Weerheijm, L. J. Sluys, A viscosity regularized plasticity model for ceramics, European Journal of Mechanics / A Solids 72 (July 2017) (2018) 310–328. doi:10.1016/j.euromechsol.2018.05.009.
URL https://doi.org/10.1016/j.euromechsol.2018.05.009

[35] A. Needleman, Material rate dependence and mesh sensitivity in localization problems, Computer Methods in Applied Mechanics and Engineering 67 (1) (1988) 69–85. doi:10.1016/0045-7825(88)90069-2.

[36] W. Wang, L. Sluys, R. De Borst, Interaction between material length scale and imperfection size for localisation phenomena in viscoplastic media, European Journal of Mechanics - A/Solids 15 (3) (1996) 447–464.

[37] A. Winnicki, C. J. Pearce, N. Bićanić, Viscoplastic Hoffman consistency model for concrete, Computers and Structures 79 (1) (2001) 7–19. doi:10.1016/S0045-7949(00)00110-3.

[38] Dynaflow Research Group, Jem-jive.
URL http://jem-jive.com

[39] D. Sulsky, Z. Chen, H. L. Schreyer, A particle method for history-dependent materials, Computer Methods in Applied Mechanics and Engineering 118 (1-2) (1994) 179–196. doi:10.1016/0045-7825(94)90112-0.

[40] F. Li, J. Pan, C. Sinka, Modelling brittle impact failure of disc particles using material point method, International Journal of Impact Engineering 38 (7) (2011) 653–660. doi:10.1016/j.ijimpeng.2011.02.004.
URL http://dx.doi.org/10.1016/j.ijimpeng.2011.02.004

[41] L. B. Lucy, A numerical approach to the testing of the fission hypothesis, The Astronomical Journal 82 (12) (1977) 1013–1024.

[42] J. J. Monaghan, Smoothed particle hydrodynamics, Annual Review of Astronomy and Astrophysics 30 (september) (1992) 543–574. doi:10.1088/0034-4885/68/8/R01.
URL http://iopscience.iop.org/0034-4885/68/8/R01$\delimiter"026E30F$nhttp://arxiv.org/abs/1007.1245

[43] R. Clegg, Development and application of a Rankine plasticity model for improved prediction of tensile cracking in ceramic and concrete materials under impact, 14th DYMAT Technical Meeting.
URL http://hsrlab.gatech.edu/AUTODYN/papers/paper143.pdf

[44] E. Strassburger, Visualization of Impact Damage in Ceramics Using the Edge-On Impact Technique, International Journal of Applied Ceramic Technology 1 (3) (2005) 235–242. doi:10.1111/j.1744-7402.2004.tb00175.x.
URL http://doi.wiley.com/10.1111/j.1744-7402.2004.tb00175.x

[45] W. Riedel, S. Hiermaier, K. Thoma, Transient stress and failure analysis of impact experiments with ceramics, Materials Science and Engineering B: Solid-State Materials for Advanced Technology 173 (1-3) (2010) 139–147. doi:10.1016/j.mseb.2009.10.038.
URL http://dx.doi.org/10.1016/j.mseb.2009.10.038

[46] H. Zolghadr Jahromi, B. A. Izzuddin, Energy conserving algorithms for dynamic contact analysis using newmark methods, Computers and Structures 118 (2013) 74–89. doi:10.1016/j.compstruc.2012.07.012.

[47] J. Ning, H. Ren, T. Guo, P. Li, Dynamic response of alumina ceramics impacted by long tungsten projectile, International Journal of Impact Engineering 62 (2013) 60–74. doi:10.1016/j.ijimpeng.2013.06.006.
URL http://dx.doi.org/10.1016/j.ijimpeng.2013.06.006

[48] H. L. Ren, X. F. Shu, L. I. Ping, Numerical and experimental investigation of the fracture behavior of shock loaded alumina, Science China: Physics, Mechanics and Astronomy 53 (2) (2010) 244–252. doi:10.1007/s11433-009-0267-y.

[49] S. Feli, M. R. Asgari, Finite element simulation of ceramic/composite armor under ballistic impact, Composites Part B: Engineering 42 (4) (2011) 771–780. doi:10.1016/j.compositesb.2011.01.024.
URL http://linkinghub.elsevier.com/retrieve/pii/S1359836811000527

[50] P. Lundberg, Interface Defeat and Penetration : Two Modes of Interaction between Metallic Projectiles and Ceramic Targets, Comprehensive Summaries of Uppsala Disserations from the Faculty of Science and Technology.

[51] R. Krashanitsa, S. Shkarayev, Computational Study of Dynamic Response and Flow Behavior of Damaged Ceramics, in: 46th AIAA/ASME/ASCE/AHS/ASC Structures, Structural Dynamics and Materials Conference, 2005, pp. 1–8. doi:10.2514/6.2005-1847.
URL http://arc.aiaa.org/doi/10.2514/6.2005-1847

[52] C. Swaroop, A. K. Srivastava, Numerical Analysis of Ballistic Performance of Curved Ceramic, in: Proceeding of STME-2013, International Conference on Smart Technologies for Mechanical Engineering, Delhi, 2013.

[53] A. Tasdemirci, I. W. Hall, Numerical and experimental studies of damage generation in multi-layer composite materials at high strain rates, International Journal of Impact Engineering 34 (2) (2007) 189–204. doi:10.1016/j.ijimpeng.2005.08.010.

[54] D. E. Grady, Dynamic Properties of Ceramic Materials, Tech. Rep. February, Sandia National Laboratories, Albuquerque (1995).

[55] T. J. R. Hughes, Generalization of Selective Integration Procedures to Anisotropic and Nonlinear Media, Short Communications 15 (9) (1980) 1413–1418. doi:10.1002/nme.1620150914.

[56] B. G. Compton, E. A. N. Gamble, V. S. Deshpande, F. W. Zok, Damage development in an armor alumina impacted with ductile metal spheres, Journal of Mechanics of Materials and Structures 7 (6).

[57] K. A. Iyer, Relationships between multiaxial stress states and internal fracture patterns in sphere-impacted silicon carbide, International Journal of Fracture 146 (1-2) (2007) 1–18. doi:10.1007/s10704-007-9108-z.

[58] E. K. Öberg, J. Dean, T. W. Clyne, Effect of inter-layer toughness in ballistic protection systems on absorption of projectile energy, International Journal of Impact Engineering 76 (2015) 75–82. doi:10.1016/j.ijimpeng.2014.09.006.

[59] A. F. Kirstein, R. M. Woolley, Symmetrical bending of thin circular elastic plates on equally spaced point supports, Journal of Research of

the National Bureau of Standards, Section C: Engineering and Instrumentation 71C (1) (1967) 1–10. doi:10.6028/jres.071C.002.
[60] C. H. Hsueh, C. R. Luttrell, P. F. Becher, Modelling of bonded multilayered disks subjected to biaxial flexure tests, International Journal of Solids and Structures 43 (20) (2006) 6014–6025. doi:10.1016/j.ijsolstr.2005.07.020.
[61] B. J. de Smet, P. W. Bach, H. F. Scholten, L. J. M. G. Dortmans, G. de With, Weakest-link failure predictions for ceramics III: Uniaxial and biaxial bend tests on alumina, Journal of the European Ceramic Society 10 (2) (1992) 101–107. doi:10.1016/0955-2219(92)90124-V.
[62] T. J. Holmquist, G. R. Johnson, C. a. Gerlach, An improved computational constitutive model for glass, Philosophical Transactions of the Royal Society A: Mathematical, Physical and Engineering Sciences 375 (2085). doi:10.1098/rsta.2016.0182.
[63] H. C. Heard, C. F. Cline, Mechanical behaviour of polycrystalline BeO, Al2O3 and AlN at high pressure, Journal of Materials Science 15 (8) (1980) 1889–1897. doi:10.1007/BF00550614.
[64] E. B. Zaretsky, V. E. Paris, G. I. Kanel, A. S. Savinykh, Evidences of ductile and brittle responses of ceramics under shock wave loading, Journal de Physique IV2 110 (2003) 917–922.
[65] E. B. Zaretsky, V. E. Paris, G. I. Kanel, A. S. Savinykh, Evidence of Ductile (Alumina) and Brittle (Boron Carbide) Response of Ceramics Under Shock Wave Loading, Ceramic Transactions 151 (2003) 105–115. arXiv:arXiv:1011.1669v3, doi:10.1017/CBO9781107415324.004.